**UNIVERSITY OF LATVIA**

FACULTY OF MEDICINE


**Līga Kunrade**

# DEVELOPMENT OF MESENCHYMAL STEM CELL IN VITRO MODELS FOR TISSUE REGENERATION AND ANTI-TUMOR DRUG DELIVERY STUDIES

DOCTORAL THESIS

Promotion to the degree of Doctor of Basic Medical Science including Pharmacy

Subfield of Pharmaceutical Pharmacology

Riga, 2020

The doctoral thesis study was carried out at the Pharmacy study program, Faculty of Medicine, University of Latvia, from 2015 to 2019.

The thesis consists of eight chapters.
Form of the thesis: summary of publications.
Supervisor: **Prof. Dr. biol., Una Riekstiņa**

Reviewers:
1) Prof. *Dr. Med.* Baiba Jansone, University of Latvia
2) *Dr. Pharm.* Edgars Liepiņš, Latvian Institute of Organic Synthesis
3) Assoc. Prof., *Dr. Med.* Augustas Pivoriūnas, Vilnius Gediminas Technical University

The thesis will be defended at the public session of the Doctoral Committee of Medicine and Health Sciences on September 25th 2020 at University of Latvia, House of Science, Jelgavas Street 3, room 207, at 13.00.

The thesis is available at the Library of the University of Latvia, 19 Raina blvd., Riga, Latvia.

This thesis is accepted for the commencement of the degree of Doctor of Basic Medical Science including Pharmacy on 11th of June 2020 by the Doctoral Committee of Medicine and Health Sciences, University of Latvia.

Chairman of the Doctoral Committee _____/
Dr. med., Professor **Valdis Pīrāgs**

Secretary of the Doctoral Committee _____/
Dr. biol., Associated Professor **Līga Plakane**

SUMMARY

Mesenchymal stem cells (MSCs) are multipotent adult stem cells found in the stroma of a variety of tissues in the adult body. MSCs possess regenerative and immunomodulatory properties that make them an attractive target for the development of cell-based treatments. MSCs are easily accessible, expandable and scalable for production at industrial levels.

The goal of the thesis was to develop MSC *in vitro* model systems to study tissue regeneration and anti-tumor drug delivery.

We observed that MSCs in undifferentiated state express neuroectodermal markers and therefore could be prone to differentiation into neuroglial cell types. A method for MSC differentiation into peripheral glia cells was adopted. After differentiation, MSCs demonstrated an increased myelin binding protein (MBP) expression and brain-derived neurotrophic factor (BDNF) secretion characteristic to Schwann cell-like cells (SC-lcs). The established *in vitro* model was used for screening of sigma 1 receptor (S1R) ligand effects on glial differentiation. The results showed that S1R antagonist NE-100 inhibited MBP expression in SC-lcs indicating that S1R could be involved in myelinating Schwann cell functions.

Owing to their tumor tropism, MSCs have been suggested as potential drug delivery vehicles for anti-tumor therapy. *In vitro* model was used to test whether MSCs could uptake nanoparticles and deliver them to tumor cells. We chose quantum dots 655 (QD655) to study the delivery of nanoparticles by MSCs. 3D co-culture model system, consisting of MSCs and tumor cells, was developed. We demonstrated that QD-loaded MSCs can deliver nanoparticles to non-metastatic and metastatic breast cancer cells. Importantly, a higher delivery efficiency was observed to metastatic breast cancer cells.

Finally, MSC trilineage differentiation model was used to study the effect of plant-derived polyphenols, namely anthocyanidins, on MSC differentiation into adipocytes, chondrocytes and osteocytes *in vitro*. Remarkably, we saw that delphinidin inhibited adipogenesis, malvidin stimulated osteodifferentiation, whereas cyanidin and delphinidin promoted chondrogenesis *in vitro*. These results indicate that plant-derived anthocyanidins could be further studied *in vivo* as part of a healthy diet or food supplements with obesity, osteoarthritis and osteoporosis preventing effect.

**Keywords:** mesenchymal stem cells, Schwann cells, osteogenesis, adipogenesis, chondrogenesis, tumor, targeted delivery.

KOPSAVILKUMS

Mezenhimālās cilmes šūnas (MCŠ) ir multipotentas pieaugušo cilmes šūnas, kas atrodamas dažādu cilvēka audu un orgānu stromā. MCŠ piemīt reģeneratīvas un imūnmodulējošas īpašības, kas tās padara piemērotas uz šūnām balstītu zāļu izstrādei. MCŠ ir viegli pieejamas, pavairojamas un piemērojamas ražošanai industriālos daudzumos.

Doktora darba mērķis bija izveidot MCŠ *in vitro* modeļsistēmas audu reģenerācijas un pretvēža zāļu piegādes pētījumiem.

Pētījumu gaitā mēs novērojām, ka nediferencētas MCŠ ekspresē neiroektodermas marķierus un tādējādi tās varētu būt piemērotas diferenciācijai par neiroglijas šūnām. Lai to pārbaudītu, mēs izveidojām metodi MCŠ diferenciācijai par perifērās glijas šūnām. Pēc diferenciācijas MCŠ bija paaugstināta mielīna saistošā proteīna (MBP) ekspresija un no smadzenēm iegūtā neirotrofā faktora (BDNF) sekrēcija, kas raksturīga Švāna šūnām, apliecinot, ka diferenciācijas rezultātā ir iegūtas Švāna šūnām-līdzīgas šūnas (SC-lc). Mēs izmantojām izveidoto *in vitro* modeli, lai analizētu sigma 1 receptora (S1R) ligandu ietekmi uz glijas diferenciāciju. Rezultāti uzrādīja, ka S1R antagonists NE-100 inhibē MBP ekspresiju SC-lc, liecinot par to, ka S1R varētu būt iesaistīts mielinējošu Švāna šūnu funkciju nodrošināšanā.

MCŠ raksturīgā audzēju tropisma dēļ, tās varētu kalpot kā zāļu piegādes vektors pretvēža terapijā. Mēs izveidojām *in vitro* modeli, lai pārbaudītu, vai MCŠ spēj uzņemt nanodaļiņas un nogādāt tās uz audzēja šūnām. Mēs izveidojām 3D kopkultūras modeļsistēmu, kas sastāvēja no MCŠ un vēža šūnām, un pierādījām, ka nanokristālus QD655 uzņēmušās MCŠ spēj nogādāt nanodaļiņas uz ne-metatstātiskām un metastātiskām krūts vēža šūnām. Augstāka piegādes efektivitāte tika novērota uz metastātiskajām krūts vēža šūnām.

Noslēgumā mēs izmantojām MCŠ trīs līniju diferenciācijas modeli, lai pētītu augu izcelsmes polifenolu, antocianidīnu, ietekmi uz MCŠ diferenciāciju par adipocītiem, hondrocītiem un osteocītiem *in vitro*. Mēs novērojām, ka delfinidīns inhibē adipoģenēzi, malvidīns stimulē osteodiferenciāciju, bet cianidīns un delfinidīns veicina hondroģenēzi *in vitro*. Šie rezultāti liecina par to, ka augu izcelsmes antocianidīnus varētu pētīt *in vivo* kā veselīgas diētas piedevas vai uztura bagātinātājus ar aptaukošanos, osteoartrītu un osteoporozi kavējošu efektu.

**Atslēgas vārdi:** mezenhimālās cilmes šūnas, Švāna šūnas, osteoģenēze, adipoģenēze, hondroģenēze, audzējs, mērķēta zāļu piegāde.

## Table of Contents

# ABBREVIATIONS

2D – two dimensional

3D – three dimensional

BDNF – brain-derived neurotrophic factor

BMP-2 – bone morphogenic protein 2

bFGF – basal fibroblast growth factor

CAF – carcinoma associated fibroblasts

CNS – central nervous system

Col1a1 – collagen type 1, alpha 1

Col2a1 – collagen type 2, alpha 1

CPZ - chlorpromazine

CytD - cytohalasin D

EIPA - 5-(N-ethyl-N-isopropyl) amiloride

EGF – epidermal growth factor

EpCAM - epithelial cell adhesion molecule

FABP4 – fatty acid binding protein 4

FBS – fetal bovine serum

GDNF – glia-derived growth factor

GLP-1 – glucagon-like peptide 1

IFN - interferon

IL – interleukin

LPL – lipoprotein lipase

MBP – myelin basic protein

MSCs – mesenchymal stem cells

NPs - nano-particles

NCSC – neural crest stem cells

PNS – peripheral nervous system

PolyHEMA - poly-2-hydroxyethyl methacrylate

QDs – quantum dots

RT-PCR – reverse transcriptase polymerase chain reaction

SC-lcs – Schwann cell-like cells

SSEA-4 – stage specific embryonic antigen 4

SPM – Schwann precursor medium

S1R – sigma 1 receptor

TGF-β1 – tumor growth factor beta 1

VEGF – vascular endothelial growth factor

## Goals and objectives of the thesis

**The goal of the thesis** was to develop mesenchymal stem cell *in vitro* model systems to study tissue regeneration and anti-tumor drug delivery.

**Objectives of the thesis**:

1) to characterize the MSC differentiation into peripheral glia in defined media conditions;
2) to use the established MSC glial differentiation protocol for pharmacologically active compound screening;
3) to establish an *in vitro* model for nanoparticle biocompatibility and uptake analysis in MSCs;
4) to develop a three-dimensional cell co-culture model to study the nanoparticle delivery from MSCs to tumor cells;
5) to evaluate the natural compound effect on MSC differentiation ability into adipocytes, chondrocytes and osteocytes *in vitro*.

**Theses for defense:**

1) MSCs can be differentiated into peripheral glia;
2) MSC-derived peripheral glia *in vitro* model system can be used to study pharmacologically active compound screening;
3) MSCs *in vitro* model can be used to study MSC and nanoparticle interaction;
4) MSCs can deliver nanoparticles to tumor cells in an *in vitro* three-dimensional co-culture model system;
5) MSCs can be used to study the effect of natural compounds on the differentiation into adipocytes, osteocytes and chondrocytes *in vitro*.

# 1. LITERATURE OVERVIEW

## 1.1. Mesenchymal stem cells

Mesenchymal stem cells (MSCs) are multipotent adult stem cells found in the stroma of a variety of tissues in the adult body. These cells have the capacity to self-renew and differentiate into other cell types, for example, osteocytes, adipocytes, chondrocytes and muscle cells. Historically osteogenic stem cells capable of osteodifferentiation, when transplanted ectopically in the kidney capsule were discovered in bone marrow by Friedenstein 1966 (Friedenstein et al. 1966). Later it was shown that fibroblast-like cells from bone marrow form clonogenic colonies *in vitro*, called colony-forming unit fibroblasts (CFU-F). CFU-F cells demonstrated the ability to differentiate into osteocytes, chondrocytes and adipocytes *in vitro* (Friedenstein et al. 1970). The term MSCs was first introduced by Arnold Caplan in a review paper in 1991 (Caplan 1991). The name "mesenchymal" originates from the term "mesenchyme" that is synonymous to embryonic connective tissue. The multilineage differentiation potential of single bone marrow MSC colonies was discovered by Pittenger et al. 1999 (Pittenger et al. 1999). According to the definition of The International Society for Cell & Gene Therapy (ISCT), MSCs are characterized by three criteria: adherence to the plastic surface, expression of surface markers CD73, CD90, CD105, lack of hematopoietic markers CD14, CD34, CD45 and HLA-DR, and ability to differentiate into adipocytes, osteocytes and chondrocytes (Fig. 1) (Dominici et al. 2006).

In 2019 ISCT issued a position statement defining that MSCs are not equivalent to mesenchymal stromal cells. The former refers to a stem cell population with a progenitor cell functionality and differentiation while the latter refers to a cell population with a prominent secretory, immunomodulary and homing properties (Viswanathan et al. 2019). Due to the fact that experiments and papers used in this thesis have been published before ISCT statement 2019, the term MSCs will be used in the thesis. Today several MSC containing medicinal products are authorized in several countries, including Prochymal (Osiris, approved in Canada), Alofisal (TiGenix and Takeda, approved in Europe), Temcell (JCR Pharmaceuticals, approved in Japan), HeartSheet (Terumo, approved in Japan), Cartistem (Medipost, approved in South Korea), and Hearticellgram-AMI (FCB-Pharmicell, approved in South Korea). Approximately 9000 clinical trials are on-going according to clinicaltrials.gov. Taking into account the fast development in the cell therapy and tissue engineering field, it is predicted that 86 total MSC products could be on the market by 2040 (Olsen et al. 2018).

MSCs were originally isolated from bone marrow, but since then they have been found at various tissue types including adipose tissue, dental tissue, skin, umbilical cord and other (Riekstina et al. 2009, Chen et al. 2015). MSCs can be cultured long-term *in vitro* without any changes in function, morphology, karyotype and phenotype (Volarevic et al. 2014). MSCs can be expanded as an adherent culture to great numbers, cells exhibit robustness and ability to successfully survive freeze-thawing cycle which make them suitable for storage and transportation. MSCs from various tissue sources are not completely identical and exert differences in cell surface marker expression, proliferation rate and differentiation capacity. It is not clear though whether these differences would cause any alterations in therapeutic efficacy since no side by side clinical comparison has been conducted (Hoogduijn and Lombardo 2019). It has been demonstrated that neonatal MSCs derived from umbilical cord or Wharton's jelly have a higher proliferative potential and delayed senescence in comparison to adult tissue derived MSCs (Hass et al. 2011). MSCs show differences in surface marker expression. Markers Stro-1, CD271, stage-specific embryonic antigen 4 (SSEA-4), CD146 are all present in MSCs derived from bone marrow and dermis. Adipose tissue-derived MSCs lack the expression of Stro-1 and SSEA-4 while MSCs from dental pulp, synovial membrane and placenta lack the expression of CD271. This indicates that there is no sole marker that is truly MSC-specific. Surface marker expression can vary in response to media composition, disease conditions, inflammation, culture confluency, growth factors and cytokines (Lv et al. 2014).

Crucial feature for MSC therapeutic potential is the cell secretome. It is enriched in different soluble factors including cytokines, chemokines, immunomodulatory molecules and growth factors (Fig. 1). MSCs secrete extracellular vesicles which can contain paracrine factors. The use of cell secretome alone has been suggested to develop cell-free therapeutic strategies (Ferreira et al. 2018).

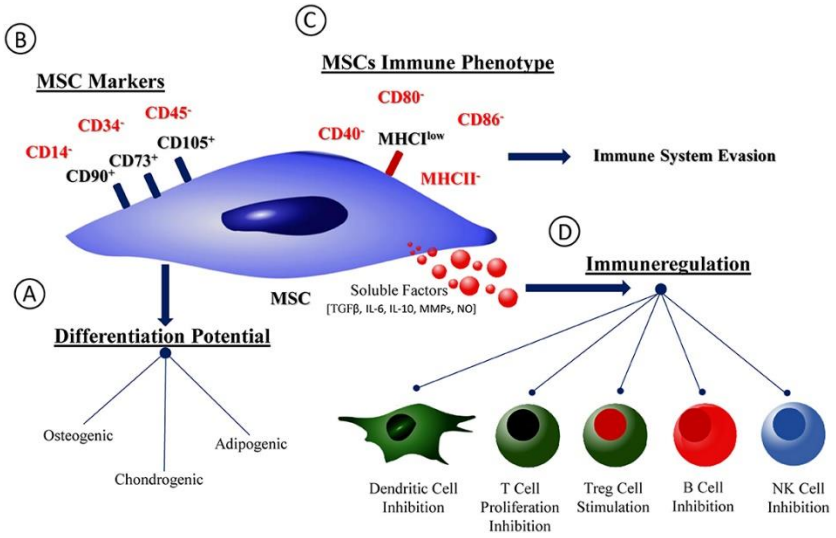


Fig.1. **MSC phenotype, differentiation potential, and immunological properties. Schematic representation of MSC phenotype and immunological profile. (A) MSC capacity of differentiation into osteogenic, chondrogenic and adipogenic lineages. (B) Characteristic MSC marker expression profile. (C) MSC immunological profile. (D) Soluble factor families produced by MSCs and profile of interaction with immune cells (Ferreira et al. 2018).**

### 1.1.1. Mesenchymal stem cell clinical application

The first infusions of MSCs into cancer patients has begun already in 1993. After intravenous infusion of MSCs, no adverse reactions and toxicity were observed (Lazarus et al. 1995). Administration of MSCs have shown an excellent safety profile which has led to over 950 clinical trials which are currently carried out to investigate MSC clinical applications (Pittenger et al. 2019). In clinical trials allogenic and autologous source MSCs are used and both have shown to yield sufficient cell number for therapeutic application. It has been demonstrated that the count of colony forming units of MSCs decreases if the donor is over 20 years old (Stolzing et al. 2008). Cell populations isolated from older donors have shown to contain more apoptotic cells and have a slower proliferation rate comparing to cells obtained from younger donors (Andrzejewska et al. 2019).

The route of the MSC administration depends on the therapeutic indication. For immunological implications, intravenous administration is the first choice route, while for wound healing a local injection is preferred. MSCs can be seeded on transplantable scaffolds or implanted as cartilaginous templates that differentiate into bone tissue after implantation (Hoogduijn and Lombardo 2019).

MSCs have very distinct immunomodulatory properties (Fig. 1). MSCs have the ability to interact and regulate the function of the majority of immune system cells such as neutrophils, natural killer cells, macrophages, lymphocytes, mast cells and dendritic cells (Andrzejewska et al. 2019). MSCs are capable of arresting B-cell proliferation, inhibit chemotaxis, up-regulate antibody production, inhibit T cell proliferation, decrease the pro-inflammatory cytokine production, decrease the cytotoxic effects of T killer cells, up-regulate phagocytosis genes in macrophages and down-regulate inflammatory cytokine secretion in macrophages (Saeedi et al. 2019). Novel hypothesis propose that MSCs could exert a better therapeutic potential by inducing regulatory and regenerative phenotype in phagocytic cells than by optimizing the secretory profile and migratory capacity of MSCs themselves (Hoogduijn and Lombardo 2019).

MSCs can differentiate into ectodermal, mesodermal and endodermal lineages and the fate of differentiation can be directed by different growth media and media supplements (Ullah et al. 2015). One of the main criteria for MSCs is the ability to differentiate into adipocytes, osteocytes and chondrocytes, however it has been demonstrated that MSCs can also be a source for other cell types. Addition of 5-azacytidine induce MSC mesodermal differentiation into muscle cells including cardiomyocytes (Andrzejewska et al. 2019). Two stage differentiation with epidermal growth factor (EGF), basal fibroblast growth factor (bFGF), nicotinamide and next stage with oncostatin, dexamethasone, insulin, transferrin and selenium has resulted in the generation of endodermal lineage hepatocytes (Lee et al. 2004). MSC differentiation into ectodermal lineage nerve cells has been demonstrated by the use of beta-mercaptoethanol (βME) and nerve growth factor (NGF) (Naghdi et al. 2009). It has been demonstrated that mesodermal progenitors isolated from perinatal and postnatal tissue have a different intrinsic differentiation potential *in vivo* which indicates that MSCs with identical differentiation capacities does not exist (Sacchetti et al. 2016).

MSCs are investigated as cell therapy candidates mainly due to their differentiation capacity, migration potential and immunomodulatory properties. MSCs are shown to migrate towards the sites of inflammation and even tumors *in vivo* (Kim and Cho 2013). Additionally to migration, MSCs can home in the injured area, differentiate into local components and improve the tissue regeneration by the secretion of biologically active molecules i.e. chemokines and cytokines (Fu et al. 2019).

### 1.2. Mesenchymal stem cells in neuroregeneration

Due to limited central and peripheral nervous system (CNS, PNS) self-regeneration capacity, exogenous stem cells are seen as viable alternative for the treatment of neurodegenerative diseases. MSCs possess an intrinsic plasticity that enables them to differentiate into mesodermal and neuroectodermal lineages. Though, the ability of MSCs to differentiate directly towards functional neurons has been under an extensive debate (Takeda and Xu 2015). Reported MSC neural differentiation studies mostly demonstrate neuron-like morphology, expression of neural markers and formation of synaptic structures, however functional neuronal properties such as synaptic transmission, membrane potential and functional action potential is usually missing (Urrutia et al. 2019). The underlying mechanisms of MSC positive therapeutic effect on neuroregeneration is not completely understood. Some of the hypothesis are: differentiation of MSCs into mature neurons/glia, immunoregulatory effect on immunoreactive host cells, neuroprotective effect of MSCs, remyelination carried out by activation of neural and oligodendrocyte progenitor cells (Rivera and Aigner 2012).

MSC ability to differentiate into neurons could renew lost neural and glial cells in therapeutic indications such as neurodegenerative diseases or spinal cord injuries (Saeedi et al. 2019). The neurotrophin levels in CNS disease patients significantly decrease and are associated with neuron damage, therefore increasing the neurotrophin levels or at least maintaining their physiological levels is of a high therapeutic value (Abbasi-Kangevari et al. 2019). Use of βME and NGF has shown to induce MSC differentiation into cholinergic neurons with the characteristic marker expression profile such as neurofilament-160 and -200, choline acetyltransferase and synapsin (Naghdi et al. 2009, Andrzejewska et al. 2019). Also use of retinoic acid (RA), insulin, bFGF, EGF, valproic acid and hydrocortisol has been associated with the MSC differentiation into nerve cells that express the characteristic markers such as nestin, β-III tubulin, microtubule associated protein 2 (MAP-2) and enolase 2 (ENO-2) (Anghileri et al. 2008, Andrzejewska et al. 2019). When comparing different marker expression profile in MSCs from bone marrow, adipose tissue, dermis and heart, the highest nestin expression was observed in MSCs from dermal tissue indicating that this source might be more prone to neurodifferentiation (Riekstina et al. 2009).

MSCs are considered for spinal cord injury treatment due to the ability to promote neuron survival through synthesis of neurotrophic and angiogenic factors that support the growth of axons (Mukhamedshina et al. 2019). Promising results *in vivo* have been obtained in rat sciatic nerve damage model where MSC injections improved the nerve regeneration after the injury by

enhancing axon count at the injury site (Cooney et al. 2016). The sciatic nerve injury model has been used also to assess the regenerative potential of adipose tissue-derived MSCs embedded in fibrin glue. In this way, cells demonstrated a neuroprotective effect in dorsal root ganglion sensory neurons, stimulated axon growth, myelination, improved the post-traumatic changes in the sensory neuron, stimulated nerve angiogenesis and motor function recovery (Masgutov et al. 2019). MSCs secrete neurotrophic factors and anti-inflammatory cytokines such as brain-derived neurotrophic factor (BDNF), glia-derived neurotrophic factor (GDNF), NGF, tumor growth factor- β1 (TGF-β1), vascular endothelial growth factor (VEGF), interleukin-6 (IL-6), IL-10 which promote neurogenesis, neuroprotection and ensure immunomodulation in astrocytes, neurons and oligodendrocytes (Colpo et al. 2015, Saeedi et al. 2019). Neurotrophic factor secreting bone marrow-derived MSCs were investigated in a phase I/II clinical trial in patients with amyotrophic lateral sclerosis. The use of autologous MSCs in this study was concluded to be safe and a decrease in disease progression was observed indicating clinical benefits (Petrou et al. 2016).

Although MSC neurodifferentiation capacity has been widely explored, less emphasis has been put on differentiation into and impact on glial cell types. Bone marrow MSCs transplanted into cerebrospinal fluid or *corpus callosum* did not exert any regenerative effects in experimental autoimmune encephalomyelitis mice model (Salinas Tejedor et al. 2015). In another cuprizone-induced demyelination mouse model, bone marrow MSCs were transplanted into the lateral ventricles and secreted the soluble factors into the cerebrospinal fluid. As a result MSCs induced the recruitment of oligodendrocyte progenitor cells and increased the myelin content within *corpus callosum* over time, the newly formed myelin enveloped the demyelinated axons and increased the neural stem progenitor cell proliferation (Cruz-Martinez et al. 2016).

Schwann cells represent an important cell type for potential peripheral nerve regeneration therapies, however, they are difficult to isolate, expand and purify (Sun et al. 2018). It has been demonstrated that neural crest progenitor exposure to neuregulin and forskolin increase Schwann cell numbers and therefore these compounds are mostly used to induce the Schwann cell-like phenotype. Neuregulin promotes the generation of immature Schwann cells and precursor cells and stimulates their proliferation (Shah et al. 1994, Jessen et al. 2015). Two Schwann cell phenotypes are present in the body – non-myelinating and myelinating Schwann cells. They ensure metabolic and trophic support for the nerves, myelination and they are involved in the regeneration of peripheral nerves after injury (Jessen and Mirsky 2019). Schwann cell-like phenotype can be obtained from various MSC types such as bone marrow, adipose tissue, umbilical cord and skin

(Zaminy et al. 2013, Xiao and Wang 2015, Saulite et al. 2018, Sun et al. 2018). MSC-derived Schwann cell-like cells (SC-lcs) possess the characteristic bipolar and fusiform Schwann cell morphology along with the characteristic marker expression i.e. S100β, nerve growth factor receptor p75 (NGFR p75), P0, glial fibrillary acidic protein (GFAP) and BDNF (Xiao and Wang 2015). It has been shown that adipose MSCs can be differentiated into cells phenotypically similar to myelinating Schwann cells which can secrete neurotrophins, promote dorsal root ganglion axon regeneration *in vitro* and repair sciatic nerve defects in rat models *in vivo* (Sun et al. 2018). Bone marrow MSC-derived SC-lcs, seeded into collagen matrix, improve the locomotor and sensory scores in rats after induced spinal cord injury. Additionally axonal regeneration and remyelination was observed (Zaminy et al. 2013).

It has been reported that SC-lcs, derived from MSCs, de-differentiate back to stem-cell-like phenotype following a differentiation medium withdrawal. Therefore further research should be carried out to confirm the stability of the MSC-derived Schwann cells for peripheral nerve regeneration therapies *in vivo* (Faroni et al. 2016).

### 1.3. Mesenchymal stem cell potential in anti-tumor therapies

Cancer is one of the leading causes of death worldwide. Due to side effects and normal cell toxicity during the convenient cancer therapies, targeted therapy approaches are directed towards cancer cells only and it increases the specificity of the treatment (Pucci et al. 2019). Owing to their tumor homing properties, MSCs are extensively studied as targeted drug delivery moieties. For this reason, different approaches are being developed (Fig. 2).

Malignant tumors are highly heterogeneous and possess a complex microenvironment consisting of cancer, immune, vascular and stromal compartments. Part of the cancer niche are carcinoma-associated fibroblasts (CAFs) derived from resident fibroblasts or tumor-infiltrating MSCs. CAFs secrete pro-inflammatory cytokines and therefore can foster tumor growth, angiogenesis and invasion by paracrine signaling (Chan et al. 2019). MSCs can potentially contribute to the tumor progression through the differentiation into CAF or the promotion of cancer stem cells (Kabashima-Niibe et al. 2013). On the other hand, bone marrow MSC-derived extracellular vesicles induced apoptosis in HepG2 and Kaposi sarcoma cells, and necrosis of SKOV3 cells when administered simultaneously in immunocompromised mice (Bruno et al. 2013). MSCs inhibited hematological malignancies *in vivo* mainly through cell cycle arrest (Lee et al. 2019). Thus the current evidence indicated a dual role of MSCs on tumor progression.

Although there are risks related to MSC pro-tumor activity, MSCs have a distinct tumor tropism or the so-called homing potential which is one of the main reasons why MSCs are considered for anti-tumor therapies. The MSC homing to tumors consists of three major steps. First, chemoattraction towards inflammation sites directed by chemotaxis towards chemokines, cytokines and hypoxia. Second, MSC adhesion to the injured cells occurs and third, MSCs infiltrate into tumor-related inflammation sites. The homing is of particular value when it comes to an tissue and injury that are not easily accessible (Kusadasi and Groeneveld 2013, Saeedi et al. 2019). Despite the high tumor tropism in *in vitro* experiments, the administration of MSCs in animals or humans leads to a quick cell accumulation in lungs, liver and spleen indicating that the vast majority of MSC-based therapeutics have limited access to the target tissue. Lung entrapment is therefore a critical challenge for MSC-based drug delivery. Another potential application is a use for the localized treatment of residual disease following surgery or radiotherapy. Local delivery would circumvent MSC homing limitation. Due to overall safety observed for MSCs in clinical trials this could be a feasible strategy (Krueger et al. 2018).

MSCs have been shown to migrate towards irradiated cells better comparing to non-radiated cells in 4TI mouse mammary tumor cells. Irradiated 4TI cells have a higher C-C chemokine receptor type 2/mitochondrial pyruvate carrier 1/C-C motif chemokine 1 precursor (CCR2/MCP-1/CCL1) expression which is thought to be an important signal for MSC attraction (Klopp et al. 2007). Therapeutic protein use in cancer treatment is often limited due to the short half-life and toxicity towards the normal cells. Interferon-beta (IFN-β) genetically modified MSCs have shown to decrease tumor growth and increase the survival in human melanoma xenograft mouse models (Studeny et al. 2002). Similar anti-tumor effects have been described with TNF-related apoptosis-inducing ligand (TRAIL-), X-linked inhibitor of apoptosis protein (XIAP-), IFN-γ, IL-2-, IL-21-modified MSCs (Chulpanova et al. 2018). MSCs could be used to deliver therapeutic proteins to the tumors. TRAIL is a tumor-cell specific cytotoxic agent. Strategies using TRAIL-modified MSCs have shown cytotoxic effects on glioblastoma cell line *in vitro,* apoptosis induction and anti-angiogenic effects in sarcoma mouse models (Tang et al. 2014, Grisendi et al. 2015). Genetically modified MSCs could be used as an effective therapeutic tool, however such a strategy could possess additional risks such as stimulation of cancer progression (Kim et al. 2010, Chulpanova et al. 2018). Therefore, a novel suicide gene induction strategy could solve this issue. MSCs co-expressing TRAIL and a suicide gene iCasp9 were shown to successfully target an aggressive

sarcoma cell line by inducing cancer death up to 80% in 24 h with an 80% elimination efficiency of modified MSCs (Rossignoli et al. 2019).

Nanomedicine is a rapidly evolving field. Several nanodrugs are currently in clinical trials and many are already approved by the Food and Drug Administration for different indications including cancer (Ventola 2017). Nanomedicine can be used for therapy and diagnostics and it is developing a platform for the delivery of cancer drugs with increased bioavailability and concentration at the tumor site (Martinelli et al. 2019). Nano particles (NPs) in the body must overcome physiological barriers such as clearance by the kidney and reticuloendothelial organs. An improvement of NP delivery efficacy can be achieved by the increase of the circulating lifecycle and by a reduced clearance (de la Torre et al. 2020). Cancer drugs can be linked to or encapsulated into biocompatible NPs. However, to ensure a directed delivery towards the tumor, a carrier is needed. MSC ability to migrate towards inflammation, damaged tissue and tumor sites *in vivo* is a promising feature for possible drug delivery to the target sites (Chulpanova et al. 2018). Different types of NPs have been reported in the literature such as organic (liposomes, polymers), inorganic (quantum dots (QDs), metallic) and carbon-based (nanotubes, fullerens) for the potential in tumor targeting and treatment (Wang et al. 2017).

To ensure the efficiency of nanoagents, a better understanding of cell and NP interaction and tumor heterogeneity is needed (de la Torre et al. 2020). The toxicological evaluation of NPs includes the *in vivo* distribution, metabolism and excretion. NP related safety concerns are linked to cell toxicity, aggregation of NPs, long-term accumulation, immunogenic behavior and hemolytic effects (Paris et al. 2019). The nanoengineered MSC homing ability is a passive accumulation. To improve tumor retention and uptake in cells, active targeting of NPs is proposed. This approach relies on the interaction between ligands conjugated on the surface of NPs and their target. Tumor cell surface receptors and secreted molecules can serve as target substrates for such an active targeting (de la Torre et al. 2020).

MSCs can incorporate small anti-tumor molecules such as paclitaxel and doxorubicin, however some downsides of this strategy include low loading capacity, rapid molecule clearance from the cells and cytotoxicity (Baxter-Holland and Dass 2018). These issues can be overcome by the encapsulation of chemotherapy drugs into the NPs. This approach requires stimuli-responsive NP-drug release strategy. Triggers can be divided into internal (pH, hypoxia) and external (temperature, ultrasound, magnetic force, electric field) stimuli (Wicki et al. 2015). Different NP biocompatibility and labelling efficiency in MSCs has been demonstrated in the literature. MSC

ability to internalize NPs makes this system suitable for labeling/tracking or drug delivery purpose (Wang et al. 2017). Gold and iron oxide NPs are shown to be safe to cells according to cell viability, however structural alterations such as degenerated mitochondria and apoptotic bodies were detected. Despite that, gold and iron NPs are biocompatible with MSCs and could be used as tracers and agents for MSC magnetic targeting (Silva et al. 2016). Silver NPs at low concentrations do not induce MSC cytotoxicity. Subtoxic concentrations of silver NPs impair the adipogenic and osteogenic differentiation of MSCs (Sengstock et al. 2014). MSCs, loaded with QDs at non-toxic concentrations, have shown to accumulate mainly in tumor and metastatic tissue in breast tumor-bearing mice (Dapkute et al. 2017).

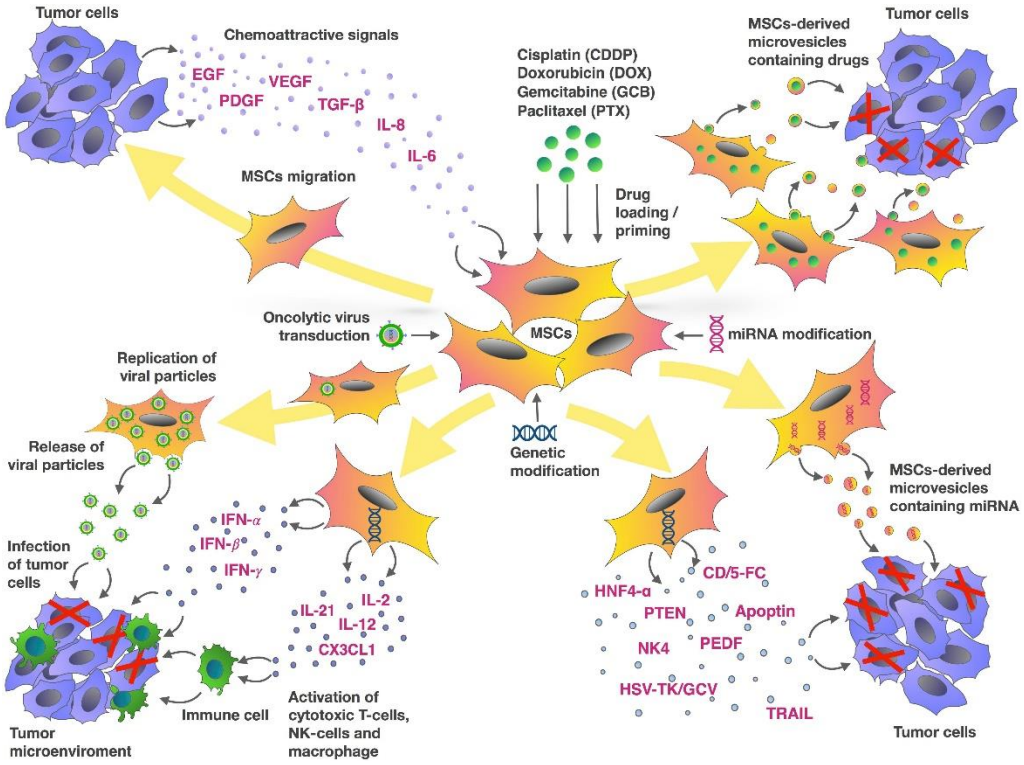


2**. MSC and tumor cell interaction as an MSC-based approach for cancer therapy. The chemotactic movement of MSCs toward a tumor niche is driven by soluble factors. Genetic modification of MSCs can be used to deliver a range of tumor-suppressing cargos directly into the tumor niche. These cargos include tumor suppressor, oncolytic viruses, immune-modulating agents and regulators of gene expression. MSCs are also capable of delivering therapeutic drugs within the tumor site. In addition to using MSCs directly, microvesicles isolated from MSCs represent an alternative approach to delivering these agents (Chulpanova et al. 2018).**

Nanomedicine technologies still need improvement to ensure safe and effective treatment for cancer patients. It is reasonable to assume that a targeted NP delivery by MSCs could be a promising strategy for therapeutic and diagnostic purposes (de la Torre et al. 2020).

### 1.4. Mesenchymal stem cells for connective tissue regeneration

MSCs play a role in tissue homeostasis and regeneration. Thus, they are of increasing interest as a treatment after injuries of connective tissue. In healthy tissue MSCs reside in the microenvironment and promote a self-renewal, however, after injuries this microenvironment is drastically changed and MSC repair ability might be impaired. For this reason, there is an interest in the design of MSC microenvironment that could guide cell differentiation and promote functional healing (Bogdanowicz and Lu 2017). Moreover, MSCs can secrete biologically active molecules that can regulate the regeneration processes (Iaquinta et al. 2019). MSCs are investigated for potential bone and cartilage regeneration in diseases like osteoporosis, osteoarthritis and even in the reduction of adipogenesis for potential obesity treatment.

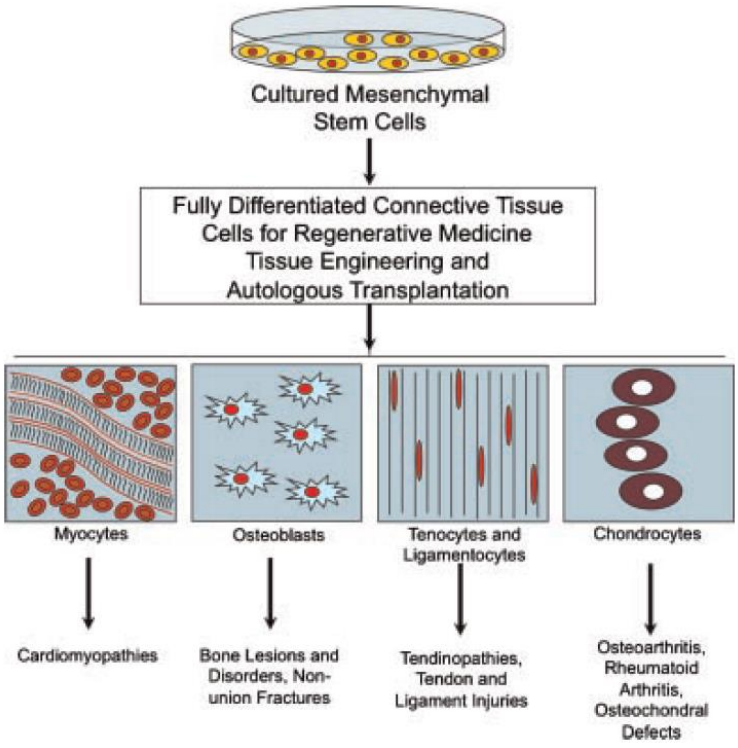


Fig. 3**. Differentiation potential of cultured MSCs. MSCs can differentiate into connective tissue and musculoskeletal cells for tissue engineering, autologous implantation/transplantation and regenerative medicine. This process involves commitment, lineage progression, differentiation and maturation (Richardson et al. 2010).**

Osteoporosis is associated with the appearance of porous bone, low bone mass, decreased bone strength and increased fracture risk (Phetfong et al. 2016). Annually more than 20 million people are affected by the loss of bone tissue (Habibovic 2017). Genetically engineered MSCs can

be used to promote osteogenesis. MSCs transduced with osteoprotegerin have shown to diminish osteoclast activation and trabecular bone loss in bone myeloma. Over-expression of telomerase reverse transcriptase (TERT) promotes osteogenic proliferation and differentiation which could be used in osteoporosis treatment (Saeedi et al. 2019). The use of exogenous MSCs immediately after an injury decreases the local inflammation while the administration of cells in intermediate periods after injury promotes bone repair due to differentiation into chondrocytes and osteoblasts and stimulation of endogenous osteoprogenitors (Grayson et al. 2015). MSCs can be administered by a systemic or local injection or by engineering techniques (Iaquinta et al. 2019). It has been demonstrated that local injection of bone marrow MSCs can improve callus formation in rats after a fracture and bone healing in a murine model (Wang et al. 2018). In larger defects alternative tissue engineering strategies, such as biomaterials together with MSCs and growth factors, might be used (Decambron et al. 2017). Studies show that a combination of extracellular matrix hydrogel and dental pulp stem cells is sufficient to induce osteogenic differentiation without the use of any osteogenic factors (Tatullo et al. 2015). In the literature different MSC-scaffold combinations are being considered for bone regeneration, such as HA/type I collagen, bioactive glass/gelatin scaffolds and others (Iaquinta et al. 2019).

In recent years, studies have shown promising potential of MSCs in cartilage lesion and osteoarthritis treatment. Osteoarthritis is manifested by articular cartilage degeneration and subchondral bone deterioration (Buckwalter et al. 2000). Similarly, as with bone regeneration also in cartilage regeneration, scaffold and scaffold-free approaches are being investigated. Percutaneous intra-articular MSC injections in anterior cruciate ligament and meniscus transection porcine models have shown that cartilage healing is induced (Lee et al. 2007). Regeneration of the meniscus and a reduction in articular chondrocyte degeneration after the MSC administration has been observed in a goat model (Murphy et al. 2003). Therapeutic effects are confirmed also in clinical trials in which patients experience a reduction of pain, regrowth of meniscus and a reduced osteoarthritis progression after MSC administration into the knee joint (Pak 2011). Pre-clinical and clinical studies comprehensively study MSC and scaffold combinations for cartilage lesions and osteoarthritis. Scaffolds include chitosan, hydrogels, collagen gel and fibrin glue. Some studies have shown that poly(lactic-co-glycolic acid) (PLGA) scaffold implanted alone can promote the regeneration of cartilage, most likely due to the adherence of endogenous stem cells (Sonomoto et al. 2016). For rheumatoid arthritis patients, whose MSCs might have an impaired differentiation capacity, a use of exogenous MSCs could be preferred to achieve a better repair of the cartilage

(Yamagata et al. 2018). These studies have verified that tissue engineering can successfully repair cartilage lesions and damage to subchondral bone (Zhang et al. 2019).

MSC role and potential targeting in obesity is being investigated in recent studies. Obesity is associated with the accumulation of excess body fat. MSCs can differentiate into adipocytes and they are a crucial source of adipocyte generation in the body (Matsushita and Dzau 2017). The addition of conditioned media from adipose-derived MSCs demonstrated the reverse of insulin resistance in preadipocyte and myoblast cell lines *in vitro*. This study suggests that MSC derived conditioned media could serve as an alternative insulin sensitizer (Shree and Bhonde 2017). Adipose-derived MSCs were injected in a high-fat diet mice and an improvement in glucose tolerance and a reduction in fatty acid infiltration in the liver was observed. This study provides a novel therapeutic strategy for the management of obesity-induced metabolic dysregulation (Shree et al. 2019). The mechanisms of MSC adipogenesis and obesity relationship should be further elucidated to discover novel MSC based therapeutic options for obesity treatment (Matsushita and Dzau 2017).

### 1.5. Future perspective of mesenchymal stem cells

Great enthusiasm and expectations have been generated since the discovery of MSCs, though the clinical progress has not been that convincing. In 2018 the first MSC product was approved for marketing authorization by the European Medicines Agency. The product contains allogenic adipose MSCs for the treatment of perianal fistulas in Crohn's disease (Stolzing et al. 2008). However, still a lot is left to investigate at the preclinical and clinical level to understand the mechanism of action, because not all patients respond to MSC therapy and clinical efficacy is observed only in approximately 50% of patients (Pittenger et al. 2019). The non-responsiveness could be explained by multiple factors such as MSC production methodology, delivery dose, cell metabolic activity, disease state and others (Caplan 2018). Cell production, delivery and efficacy in MSC-based therapies need to be enhanced and optimized to develop a more sophisticated approach in therapeutic applications and to improve the outcome. Important process steps during MSC isolation and expansion should be controlled to ensure consistency across laboratories and to achieve reproducible MSC therapy outcomes (Pittenger et al. 2019).

Novel approaches consider the cell-free MSC therapies in which only the active components of MSCs could be used for administration. MSC secretome or phagocytosis-inducing components could be sufficient to activate immunomodulatory and regenerative processes in the body

(Hoogduijn and Lombardo 2019). This approach could bypass many side effects of MSCs such as unwanted differentiation of cells and avoidance of invasive cell collection procedures (Harrell et al. 2019).

Different potential and theoretical risks of MSCs must be kept in mind before their use in therapy. Risks are associated with the type of stem cells, extrinsic risk factors such as level and type of manipulation, culturing history, handling and storage of cells, and the clinical characteristics. Clinical risks involve tumorigenic potential, immune responses and pathogen transmission by MSCs (Herberts et al. 2011). The safety considerations must take into account the personalized approach, understanding the growth regulators in differentiation, site-specific homing, bio-banking and suitable markers to isolate and characterize source-specific MSCs (Saeedi et al. 2019).

# 2. MATERIALS AND METHODS

## 2.1. Cell cultures

### 2.1.1. Mesenchymal stem cells

Human skin-derived and adipose MSCs were used in the study. Human skin samples were obtained from post-surgery materials with authorized approval from the Research Ethics Committee, Institute of Experimental and Clinical Medicine, University of Latvia (issued 04.06.2014). Skin MSC cultures were obtained as described elsewhere (Riekstina et al. 2008). All experiments were performed in compliance with the relevant laws and institutional guidelines. In this study five independent donor skin MSC cultures from passage four to passage eight were used. Cells were propagated in cultivation medium containing Dulbecco's Modified Eagle's media (DMEM)/F12 (3:1 v/v) supplemented with 10% of fetal bovine serum (FBS) and antibiotics (100 U/ml penicillin, 100 μg/ml streptomycin) (all from Sigma-Aldrich, USA).

Human adipose MSCs were purchased from the American Type Culture Collection (ATCC, PCS-500-011, Manassas, VA, USA). Human adipose MSCs were propagated in MSC Basal Medium supplemented with the MSC Growth Kit (ATCC) and antibiotics (100 U/ml penicillin, 100 μg/ml streptomycin). Cell morphology was observed with a digital inverted microscope AMG-Evos X1 (AMG, Malaga, WA, USA). 0.25% trypsin-EDTA solution (Sigma-Aldrich) was used to detach cells for experiments.

### 2.1.2. Cancer cell lines

Cancer cell lines were used in QD study. Human breast cancer cell lines MDA-MB-231 (ATCC HTB-26™) and MCF7 (ATCC HTB-22™) were propagated in DMEM supplemented with 10% FBS and penicillin/streptomycin (100 U/mL and 100 μg/mL, respectively) (complete cancer cell medium). The cells were cultured in 25 $cm^2$ polystyrene tissue culture flasks up to 90% confluence in complete cell culture medium in a humidified chamber at 37 °C with 5% $CO_2$.

## 2.2. General procedures

### 2.2.1. Mesenchymal stem cell characterization

MSC phenotype was characterized by the expression of mesenchymal markers CD90, CD73, CD105 and lack of hematopoietic markers CD34, CD45 (Table 1). Suitable isotype controls were used where appropriate. Markers were tested by flow cytometry using Guava EasyCyte 8HT flow cytometer and analyzed by ExpressPro software (Millipore, MA, USA). Antibodies are listed in Table 1.

Neuroectodermal genes *Sox10, S100b, Notch1, Integrin-α4, ErbB3, Ap2α, Integrin-α6, Nestin, Tubulin-βIII, Jun-c, p75NTR, Pax6* were analyzed by RT-PCR with a subsequent agarose gel electrophoresis. Gel imaging was done by Biospectrum imaging system UV light camera (UVP, USA).

MSC trilineage differentiation was assessed using StemPro osteogenesis, adipogenesis and chondrogenesis kits according to manufacturer's guidelines (all from ThermoFisher Scientific, Waltham, MA, USA). Supernatants from each differentiation medium were collected at the end of the experiment for further ELISA analysis. All experiments were performed in at least three biological replicates. MSC differentiation into osteocytes, adipocytes and chondrocytes was evaluated by Alizarin Red S, Oil Red O and Alcian Blue (Sigma-Aldrich, St. Louis, MO, USA) staining, respectively. The absorbance was measured with an Infinite 200 PRO plate reader and i-control software (Tecan Trading AG, Männedorf, Switzerland).

The proliferation of MSCs was analyzed by Ki67 FITC Mouse Anti-Ki67 Set according to the manufacturer's instructions (BD Bioscience, Carlsbad, CA, USA). Synchronization of the cell cycle was induced by a 24 h long serum starvation. Ki67 analysis was done by flow cytometry.

Table 1. **Antibodies used in the study. FC-flow cytometry, IF- immunofluorescence.**

| **Antibody** | **Dilution** | **Manufacturer** | Catalog nr. |
|---|---|---|---|
| Mouse anti-human tubulin-βIII primary antibody | IF 1:100 | R&D systems (Minneapolis, USA) | MAB1195 |
| Mouse anti-human GFAP primary antibody | IF 1:100 | R&D systems | MAB2594 |
| Rabbit anti-S1R primary antibody | IF 1:400 | Abcam (Cambridge, MA, USA) | ab53852 |
| Mouse anti-S100b primary antibody | IF 1:50 | BD Bioscience | 612376 |
| PE mouse anti-human CD271 primary antibody | FC 1:100 | BD Bioscience | 557196 |
| PE Mouse anti-human CD73 | FC 1:10 | BD Bioscience | 561014 |

| | | | |
|---|---|---|---|
| FITC Mouse anti-human CD90 | FC 1:100 | BD Bioscience | 555595 |
| APC mouse anti-human CD105 | FC 1:20 | BD Bioscience | 562408 |
| PE Mouse anti-human CD29 | FC 1:10 | BD Bioscience | 561795 |
| PE mouse anti-human CD34 | FC 1:10 | BD Biosciences | 555822 |
| FITC mouse anti-human CD45 | FC 1:10 | BD Biosciences | 555482 |
| FITC Mouse Anti-Ki67 | FC 1:5 | BD Bioscience | 556026 |
| FITC mouse anti-human EpCAM FITC | FC 1:5 | BD Bioscience | 347197 |
| Mouse anti-MBP (clone 2H9) primary antibody | FC 1:200 | LSBio (Seattle,WA, USA) | 556026 |
| Goat anti-mouse IgG Alexa Fluor 488 secondary antibody | FC 1:200 IF 1:400 | Thermo Fisher Scientific | A-24920 |
| Goat anti-rabbit IgG H + L Alexa Fluor 594 secondary antibody | IF 1:400 | Abcam | ab150080 |

### 2.2.2. Cell viability assay

Cell viability was analyzed by Cell Counting Kit 8 (CCK-8) (Sigma-Aldrich). A total of $5 \times 10^3$ cells per well were seeded onto 96-well plates in 100 μL of complete medium. S1R ligand PRE-084, E1R and NE-100 cytotoxicity on MSCs was tested at concentrations of 3.13, 6.25, 12.5, 25, 50, 100 and 200 μM for each drug. Cells were incubated with the ligands for 96 h. QD cytotoxicity on MSCs was tested at concentrations ranging from 0.5–64 nM with two-fold dilution. The cells were incubated with QDs for 24 and 48 h. Anthocyanidin cytotoxicity was analyzed at concentrations ranging from 25 to 200 μM. The cells were incubated with test compounds for 24 h, 48 h and 72 h. Untreated cells were used as a control, and the viability was defined as 100%. After

incubation, 10 µL of CCK-8 reagent was added to each well and incubated for 2 h at 37 °C in 5% $CO_2$ at 90% humidity. The change in the medium color corresponds to the amount of dye produced in the sample and is directly proportional to the number of viable cells. The optical density was measured using a spectrophotometer Bio-Tek ELx808 (BioTek Instruments, USA) at a wavelength of 450 nm. The background signal of substances from all of the tested concentrations was subtracted from the respective samples. Data were analyzed in Microsoft Excel and GraphPad Prism software (Graph Pad Inc., La Jolla, CA, USA).

### 2.2.3. Immunofluorescence

For immunofluorescence, cells were fixed with 4% PFA for 20 min at room temperature. Samples were then rinsed with wash buffer (1% bovine serum albumin (BSA) in PBS), permeabilized and blocked with 5% BSA and 0.3% Triton X-100 (all from Sigma-Aldrich) in PBS for 45 min at RT. Samples were incubated with primary antibodies (Table 1) according to the manufacturer's instruction. The cytoskeleton of cells was stained with methanolic Alexa Fluor488 Phalloidin (Thermo Fisher Scientific). Where necessary, cells were incubated with secondary antibody (Table 1) for 3 h at room temperature in the dark. All antibodies were diluted in wash buffer. After incubation, samples were rinsed with wash buffer three times for 5 min and mounted with ProLong Gold anti-fading mountant with DAPI (Thermo Fisher Scientific) and incubated for 24 h in the dark at RT. Cells for glial cell differentiation study were analyzed using a TILL Photonics iMIC fluorescence microscope (TILL Photonics GmbH, Gräfelfing, Germany). Images were processed using TILL Photonics Offline analysis software (TILL Photonics GmbH, Gräfelfing, Germany). Fluorescence intensity was measured as the corrected total cell fluorescence (Integrated Density - (Area of selected cell X Mean fluorescence of background readings) using ImageJ software (National Institute of Health, Bethesda, MD, USA).

### 2.2.4. Confocal microscopy

Cells for QD study were analyzed using a Nikon eclipse Ti microscope equipped with a Nikon C2 confocal system. A Nikon S Plan Fluor ELWD 40×/0.60 objective was used. For Alexa Fluor488 Phalloidin, 488 nm was used for excitation, but for DAPI and QD655, 405 nm lasers were used for excitation. To detect fluorescence for Hoechst - 447/60 nm, Alexa Fluor488 Phalloidin - 525/50 nm and QD655 - 561 LP band pass filters were used (Nikon, Japan). Each

channel was recorded separately to avoid spectral overlap. The images were analyzed using Nis-Elements C 4.13 software (Nikon, Japan).

### 2.2.5. RNA extraction

Cells were lysed using QIAzol lysis reagent (Qiagen, Hilden, Germany). Total cellular RNA was extracted from cells according to the manufacturer's guidelines. The concentration and purity of RNA were determined using a Tecan Infinite M200 Pro microplate reader. The RNA concentration was normalized to 1 μg/μl for all samples.

### 2.2.6. Real-time RT-PCR

Complementary DNA (cDNA) was synthesized using the cDNA Synthesis Kit according to the manufacturer's instructions. cDNA was amplified for 35 cycles and run on agarose gel electrophoresis. Real-time reverse transcriptase polymerase chain reaction (RT-PCR) was performed for quantitative gene expression analysis using SYBR Green fluorescent dye according to the manufacturer's instructions. All reagents for glial differentiation study were obtained from Thermo Fisher Scientific, but for anthocyanidin study from Solis Biodyne (Tartu, Estonia). Ct values were normalized to the average Ct value of the housekeeping gene, which was designated as 1. Fold change in gene expression was calculated using the ΔΔCt method (Livak and Schmittgen 2001). Primer information is summarized in Table 2.

Table 2. **Primers used in the study.**

| Gene | Sequence |
|---|---|
| *Integrin-6α* | F - ATGCACGCGGATCGAGTTT |
| | R - TTCCTGCTTCGTATTAACATGCT |
| *Nestin* | F - GGCTGCGGGCTACTGAAAAG |
| | R - AGGCTGAGGGACATCTTGAGG |
| *Tubulin-βIII* | F - ACCCCAGCGGCAACTACG |
| | R - CCAGGACCGAATCCACCAG |
| *Sox10* | F - AAGCCTCACATCGACTTCGG |
| | R - TCCATGTTGGACATTACCTCGT |
| *p75NTR* | F - CGAGGCACCACCGACAACCT |
| | R - TGGTTCACTGGCCGGCTGTT |

| | |
|---|---|
| *Pax6* | F - GGAGTGCCCGTCCATCTTTG |
| | R - GGTCTGCCCGTTCAACATCC |
| *AP2α* | F - CCACTTGGGTGCGAGACCGA |
| | R - GGGGTCGTTGACGTGGGAGT |
| *ErbB3* | F - ACACCAACTCCAGCCACGCT |
| | R - TCGGTCCCTCACGATGTCCC |
| *Integrin-4α* | F - AGAGCGCATGGCTTGGGAAG |
| | R - GAAGCGTTGGCGAGCCAGTT |
| *Notch1* | F - TTCCAGTGCGAGTGCCCCAC |
| | R - GCGTCCCCGTGTACCCTTCC |
| *JUN-c* | F - GCGCGCAGCCCAAACTAACC |
| | R - AGGAACGAGGCGTTGAGGGC |
| *S100b* | F - TGGACAATGATGGAGACGG |
| | R - ATTAGCTACAACACGGCTGG |
| *S1R* | F - GGGAGACGGTAGTACACGG |
| | R - AGGAGCGAAGAGTATAGAAGAGG |
| *GAPDH* | F - TCCCTGAGCTGAACGGGAAG |
| | R - GGAGGAGTGGGTGTCGCTGT |
| *ALPL* | F - ATCAGGGACATTGACGTGATC |
| | R - TTCCAGGTGTCAACGAGGTC |
| *Col1a1* | F - AGGGCCAAGACGAAGACATC |
| | R - AGATCACGTCATCGCACAAC |
| *Osteocalcin* | F - AGTCCAGCAAAGGTGCAGCC |
| | R - TCAGCCAACTCGTCACAGTC |
| *Runx2* | F - CAGTAGATGGACCTCGGGAA |
| | R - CCTAAATCACTGAGGCGGTC |
| *Sox9* | F - CCCATGTGGAAGGCAGATG |
| | R - TTCTGAGAGGCACAGGTGACA |
| *Col2a1* | F - GGCAATAGCAGGTTCACGTACA |
| | R - CGATAACAGTCTTGCCCCACTT |
| *Aggrecan* | F - TCGAGGACAGCGAGGCC |

| | |
|---|---|
| | R -TCGAGGGTGTAGCGTGTAGAGA |
| *Adiponectin* | F - AAGGAGATCCAGGTCTTATTGG |
| | R - ACCTTCAGCCCCGGGTAC |
| *FABP4* | F - CCTTTAAAAATACTGAGATTTCCTTCA |
| | R - GGACACCCCCATCTAAGGTT |
| *LPL* | F - TTGTGGCCGCCCTGT |
| | R - TCCTCCTCCATCCAGTTG |
| *BMP-2* | F - CACTGTGCGCAGCTTCC |
| | R - CCTCCGTGGGGATAGAACTT |
| *PPIA* | F – TCCTGGCATCTTGTCCAT |
| | R - TGCTGGTCTTGCCATTCCT |

### 2.2.7. Statistical analysis

Statistical analysis was performed using GraphPad Prism Software. The data used for analysis were representative results or the means of at least three independent experiments ± the standard error of the mean (SEM). Differences between studied groups in S1R study were statistically assessed by Student's t test, for QD study by one-way ANOVA followed by Tukey's post-hoc test and for anthocyanidin study by one-way ANOVA following the Dunnett's multiple comparison test.

## 2.3. Mesenchymal stem cell glial differentiation and characterization

Skin MSCs were used in the experiment. MSCs were differentiated into Schwann cell-like cells according to a previously described protocol (Wakao et al. 2010). The differentiation was started by changing the medium to alpha-MEM containing 1 mM βME (Sigma-Aldrich) for 24 h. Then, the medium was replaced with minimum essential medium (alpha-MEM) containing 10% FBS and 35 ng/ml RA (Sigma-Aldrich) for 3 days. Next, the medium was changed to Schwann precursor medium (SPM), alpha-MEM containing 10% FBS, 5 μM forskolin, 10 ng/ml rh-FGF-2 (Sigma-Aldrich), 5 ng/ml rh-PDGF-AA and 200 ng/ml neuregulin-1β (R&D systems, Minneapolis, USA), and cultured for additional 4 days. All media used in the study contained 100 U/ml penicillin and 100 μg/ml streptomycin. Cells were then trypsinized and collected for further analysis. Undifferentiated MSCs, cultured in the cultivation medium, were used as controls. Cell phenotype was characterized by neuroectodermal marker S100b, tubulin-βIII and GFAP expression using

immunofluorescence. Neuroectodermal gene *S100b, MBP, Sox10, p75NTR, Integrin-α6, Ap2α, Pax6, Notch1* and *Integrin-α4* expression was analyzed using RT-PCR. BDNF secretion was analyzed in cell supernatants by ChemiKine BDNF Sandwich ELISA kit (Millipore) according to the manufacturer's recommendations.

### 2.3.1. Sigma 1 receptor ligand study

The S1R selective agonist PRE-084 and selective antagonist NE-100 were obtained from Tocris (Bristol, UK). E1R ((4R,5S)-2-(5-methyl-2-oxo-4-phenyl-pyrrolidin-1-yl)-acetamide) was prepared at the Latvian Institute of Organic Synthesis according to the previously published procedure (Kalvins I 2011, Veinberg et al. 2013). PRE-084, E1R and NE-100 (each at 0.3 and 3 μM) were added to SPM on day four and cultivated with cells for four days. Concentrations were chosen according to a previously published study of S1R (Hayashi and Su 2007). Undifferentiated MSCs were incubated with S1R ligands for four days in the cultivation medium. MSCs and SC-lcs, without S1R ligand treatment, were used as negative controls. S1R expression in MSC and SC-lcs was tested by immunofluorescence. Antibodies used are summarized in Table 1. BDNF secretion was analyzed by ELISA and MBP expression was tested by flow cytometry.

## 2.4. Quantum dot study

### 2.4.1. Quantum dots

Qdot® 655 ITK™ non-targeted carboxyl-coated quantum dots were purchased from Thermo Fisher Scientific (Waltham, MA, USA). The QDs are composed of a CdSe core and ZnS shell coated with an amphiphilic polymer and functionalized with carboxylate. QD655 have an emission maximum of 655 nm. Xu et al. reported that the hydrodynamic diameter of the nanoparticles is 14.55 ± 4.157 nm and the zeta potential is −35.1 mV (Xu et al. 2016). The stock solution was prepared at a concentration of 8 μM in 50 mM borate with pH 9.0.

### 2.4.2. Preparation of nanoengineered mesenchymal stem cells

To estimate the optimal QD655 concentration for uptake experiments, $5 \times 10^4$ MSCs were allowed to adhere to 6-well tissue culture polystyrene plates and cultured in the presence of QDs from 2 nM to 32 nM concentration for 6 h in complete or serum-free medium. The cells were then harvested by trypsinization and resuspended in 200 μl PBS for further studies. QD uptake was

confirmed by flow cytometry. Nano-engineered MSCs were prepared by incubation with 8 nM QD655 for 6 h, after which, the medium was changed.

### 2.4.3. Endocytosis pathway analysis

To analyze the pathway of QD uptake in MSCs, five endocytosis inhibitors were selected: the clathrin pathway inhibitor chlorpromazine (CPZ), phagocytosis inhibitor cytohalasin D (CytD), macropinocytosis inhibitor 5-(N-ethyl-N-isopropyl) amiloride (EIPA) (Cayman Chemical, USA), caveolin/lipid raft-mediated endocytosis inhibitor nystatin and caveolin-dependent endocytosis inhibitor dynasore (all from Sigma-Aldrich, USA, unless otherwise stated). The optimal inhibitor concentration was selected using the CCK-8 viability assay. MSCs were seeded onto 8-well chamber slides with $2 \times 10^4$ cells per well in 0.5 mL of complete medium and incubated for 1 h with the respective inhibitors at the following concentrations: 40 μM CPZ, 2 μM CytD, 5 μM EIPA, 80 μM nystatin and 80 μM dynasore, at 37 °C, 5% $CO_2$ and 95% humidity. The medium was aspirated from the wells, and 16 nM QDs were added to samples in complete or serum-free medium and incubated for 6 h. The medium was aspirated and samples were rinsed with 2 mL of PBS. Control wells contained nonlabelled cells. The samples were subsequently stained with methanolic Phalloidin Alexa Fluor488 (Thermo Fisher Scientific, USA) and analyzed using confocal microscopy. Single cell borders were defined according to the Phalloidin Alexa488 staining. The mean fluorescence was measured in the middle z-section of the cell in the red channel only. As a control, the background mean fluorescence from different parts of the image was measured. The QD fluorescence intensity of single cells was calculated by subtracting the background mean intensity from the single-cell mean intensity average.

### 2.4.4. Establishment of a three-dimensional cell culture model

Poly-2-hydroxyethyl methacrylate (polyHEMA) coating was prepared as described elsewhere (Kuroda et al. 2013). In brief, the PolyHEMA solution was poured into the wells of a 24-well tissue culture polystyrene plate to cover the surface. The plate was then air-dried in a laminar airflow chamber overnight. The MSCs, MDA-MB-231 and MCF7 cells were seeded at a density $5 \times 10^4$ cells per well on polyHEMA-coated plates in the complete cell culture media. Then, the three-dimensional (3D) spheroid formation was analyzed using an EVOS XL light transmission microscope at 24, 48 and 72 h (AMG). To distinguish between cell populations in the co-culture, CD90 was chosen as a selective marker for MSCs and EpCAM was chosen as a marker for MCF7

cells. CD90 expression dynamics was analyzed in MSCs after 24, 48, 72 and 96 h of propagation in 3D culture. The spheroids were pelleted by centrifugation at 250 g for 5 min, trypsinized for 5 min at 37 °C to obtain a single cell suspension, and finally centrifuged and suspended in 100 μL of PBS. The samples were stained with or EpCAM (Table 1) according to the manufacturer's instructions and analyzed by flow cytometry.

### 2.5. Anthocyanidin effect on mesenchymal stem cell trilineage differentiation

#### 2.5.1. Anthocyanidins

Anthocyanidins malvidin chloride (≥95.0%), cyanidin chloride (≥95.0%), and delphinidin chloride (≥95.0%) were purchased from Sigma-Aldrich. Liraglutide was purchased from Toronto Research Chemicals (North York, Canada).

#### 2.5.2. Characterization of the trilineage differentiation

The MSC differentiation into osteocytes, chondrocytes and adipocytes was carried out as described in section 2.2.1. In addition, the impact of anthocyanidins on osteogenic and chondrogenic differentiation was tested by bone morphogenic protein 2 (BMP-2) secretion using BMP-2 enzyme-linked immunosorbent assay (ELISA) Kit (R&D Systems). The supernatants were collected 14 and 21 days after differentiation into chondrocytes and osteocytes, respectively. The assay was performed according to the manufacturer's instructions. The absorbance was measured at 450 nm using a Tecan Infinite 200 PRO plate reader and the i-control software.

Tissue-specific gene expression analysis was performed by real-time RT-PCR. *Adiponectin, fatty acid-binding protein 4 (FABP4), Lipoprotein lipase (LPL)* were used as adipose-specific markers. *Alkaline phosphatase* (*ALPL), Collagen type 1, alpha 1 (Col1a1), Osteocalcin*, *Runx-2* and *BMP-2* were used as osteocyte specific markers. *Sox9, Collagen type 2, alpha 1 (Col2a1), Aggrecan, Runx-2* and *BMP-2* were used as chondrocyte specific markers. Primer information is summarized in Table 2.

# 3. RESULTS

### 3.1.1. Development of *in vitro* mesenchymal stem cell glial differentiation model for pharmaceutically active compound screening

MSCs exert multipotency and therefore they could be used to develop model systems of different cell types for screening of pharmacologically active compounds.

Skin MSCs were characterized by the expression of neuroectodermal and mesenchymal markers. Flow cytometry analysis showed that skin MSCs were ≥95% positive for MSC markers CD29, CD73, CD90 and CD105 (Fig. 4, B). Moreover, MSCs in their undifferentiated state expressed a wide variety of neural, glial and neural crest stem cell (NCSC) markers. The expression of the neural crest lineage genes *Notch1*, *Integrin-4*, *ErbB3*, *Ap2α*, *Jun-c* and *p75NTR* was observed in all donor samples tested (Fig. 4, A). The NCSC genes *Sox10* and *Pax6* were expressed at low levels. *S100b* expression varied across the donors, and high expression was observed in two out of three cell lines. The expression of neural genes *Tubulin-βIII*, *Integrin-α6* and *Nestin* was present in all donor samples tested.

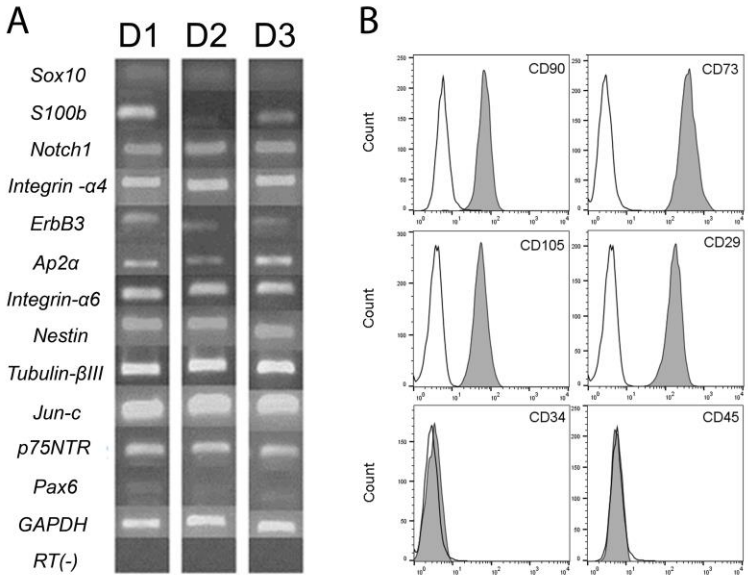


Fig. 4. **Phenotypic characterization of undifferentiated skin-derived MSCs. (A) Neuroectodermal gene expression in MSCs from three independent donors (D1, D2 and D3). (B) The expression of MSC markers CD90, CD73, CD105, CD29 and hematopoietic markers CD34 and CD45 in MSCs. Representative data are shown. Unlabeled cells (open histograms). Labelled cells (filled histograms).**

Microscopic observation revealed neurosphere formation in MSC cultures (Fig. 5, A). However, after eight days of glial differentiation, cells elongated, and bipolar morphology was

obtained. Cells spindled out from denser cell clusters and layered parallel to each other as similar to Schwann cells (Fig. 5, B), in comparison to undifferentiated MSCs which has the characteristic fibroblast morphology (Fig. 5, A). Tubulin-βIII, GFAP and S100b expression were observed in MSCs as well as in SC-lcs via immunofluorescence microscopy analysis (Fig. 5, C, D). The fluorescence signal intensity did not reveal a significant difference in GFAP and Tubulin-βIII expression between MSCs and SC-lcs. To the contrary, S100b signal was significantly upregulated ($p < 0.01$) in SC-lcs comparing to MSCs (Fig. 5, C, D). The expression of NCSC marker genes *Sox10*, *Notch1*, *Ap2α* and *Pax6* was decreased in SC-lcs as shown by real-time RT-PCR (Fig. 5, E). NCSC markers *Integrin-4α* and p*75NTR* were downregulated 2-fold ($p < 0.001$) and 3.5-fold ($p < 0.01$), respectively, in SC-lcs compared to MSCs. Nevertheless, myelin marker *myelin basic protein* (*MBP)* was significantly upregulated in SC-lcs ($p < 0.001$) (Fig. 5, E). MSCs and SC-lc culture supernatants were analyzed for BDNF secretion via ELISA. MSCs either did not secrete BDNF or secreted it in low amounts relative to SC-lcs, which showed a significant increase in BDNF secretion (Fig. 5, F).

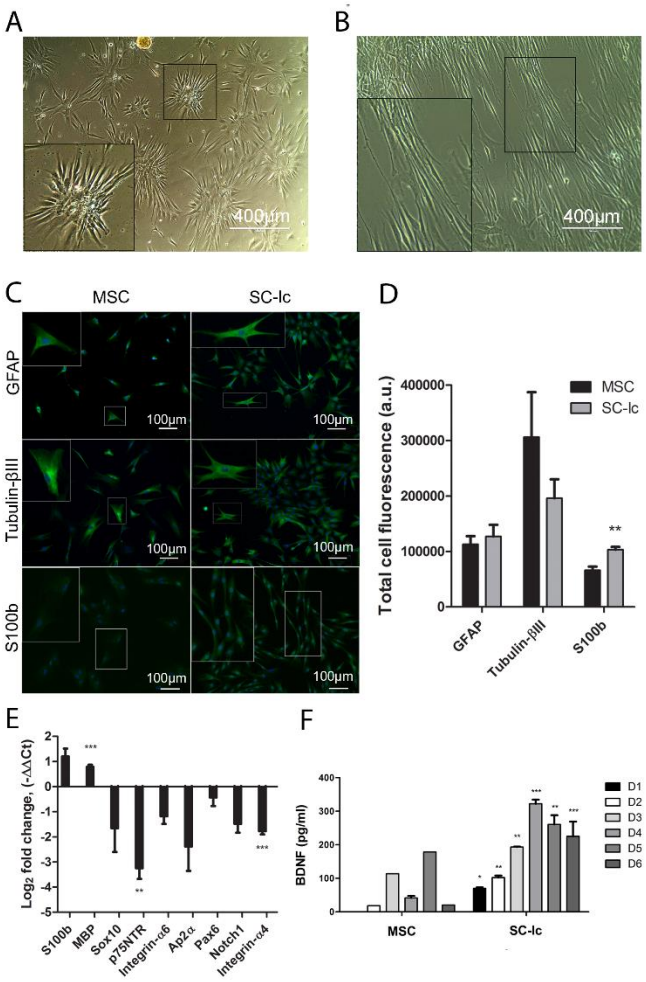


Fig. 5. **The phenotypic characterization of MSCs and SC-lcs. The morphology of (A) MSCs and (B) SC-lcs. The scale bar - 400 µm. (C) GFAP, Tubulin-βIII and S100b expression in MSCs and SC-lcs (representative data). Green - GFAP, Tubulin-βIII or S100b; blue - DAPI. The scale bar - 100 µm. (D) Quantification of GFAP, Tubulin-βIII and S100b fluorescence signal. (E) NCSC and Schwann cell gene expression in SC-lcs. Fold change was expressed as –ΔΔCt values compared to MSCs baseline expression level. (F) BDNF secretion in MSCs and SC-lcs in six independent donor cell lines (D1–D6). Statistical significance was assessed by Student's t-test. All values were corrected for multiple comparisons using Holm-Sidak method. *p-value < 0.05, **p-value < 0.01, ***p-value < 0.001.**

### 3.1.2. Screening of sigma 1 receptor ligand effect on mesenchymal stem cell glial differentiation

To evaluate the effects of S1R ligands on MSC viability, cells were treated for 96 h with PRE-084, E1R and NE-100 at concentrations ranging from 3.13 to 200 µM. A slight decrease in cell viability was observed by S1R antagonist NE-100 at 6.25 to 25 µM concentration. NE-100

concentrations higher than 25 μM induced severe concentration-dependent cell toxicity. PRE-084 and E1R had no effect on cell viability when used at concentrations of up to 200 μM (Fig. 6).

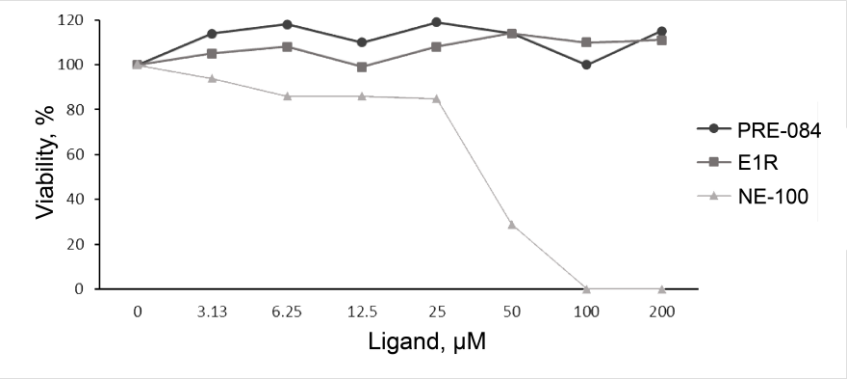


Fig. 6. **The cytotoxicity of S1R ligands. The cytotoxicity of the S1R selective agonist PRE-084, positive allosteric modulator E1R and selective antagonist NE-100 was analyzed by a colorimetric assay after 96 h treatment to evaluate their concentration-dependent effects on the viability of MSCs.**

The expression of S1R in MSCs and SC-lcs was analyzed by immunofluorescence (Fig. 7, A, B). S1R expression was observed in MSCs, however, S1R expression in SC-lc was more pronounced. Quantification of fluorescence signals revealed a significantly higher expression of S1R in SC-lcs than in MSCs (Fig. 7, B). S1R was localized in perinuclear area in MSCs, whereas in SC-lcs, S1R was evenly expressed throughout the cell cytoplasm (Fig. 7, A). S1R gene expression was increased 5.5-fold in SC-lcs comparing to MSCs (Fig. 7, C).

The expression of MBP in untreated and ligand-treated MSC and SC-lc populations was analyzed by flow cytometry. The expression of MBP in MSCs was undetectable, whereas after differentiation, 20% of SC-lcs expressed MBP (Fig. 8, A). To analyze the S1R ligand effect on MSC differentiation into SC-lcs, the selective S1R agonist PRE-084, the positive S1R allosteric modulator E1R and the selective S1R antagonist NE-100 were added at concentrations of 0.3 and 3 μM during cell differentiation. Treatment with all S1R ligands, except 3 μM NE-100, did not impact MBP expression in SC-lcs and the MBP expression level was comparable to ligand-untreated SC-lcs (Fig. 8, A). In contrast, 3 μM NE-100 inhibited the expression of MBP in SC-lcs and the expression of MBP was similar to MSCs (Fig. 8, A). In fact, SC-lcs treated with 3 μM NE-100 were the only SC-lc population in which MBP expression was at the level of undifferentiated MSCs. Next, we used ELISA to analyze the effects of S1R ligands on the secretion of BDNF in MSCs and SC-lcs (Fig. 8, B). The addition of S1R ligands had no effect on the secretion of BDNF in either MSCs or SC-lcs (Fig. 8, B).

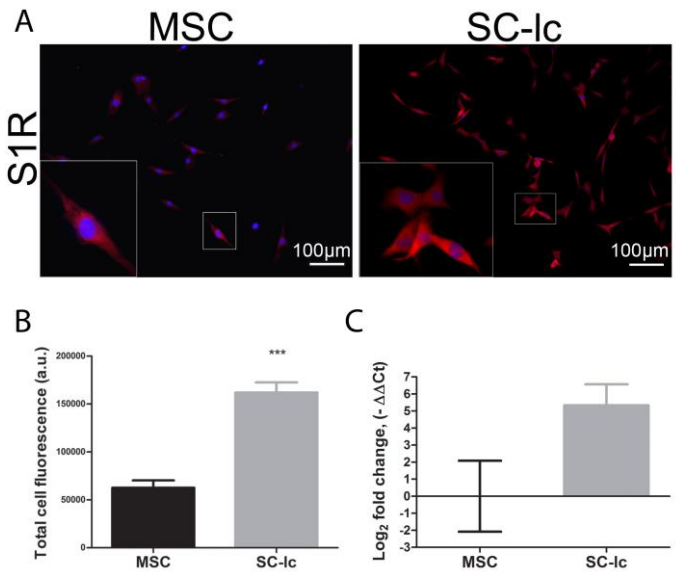


Fig. 7. **The expression of S1R in MSCs and SC-lcs. (A) Induction of S1R signal was observed in SC-lcs compared to MSCs. Red - S1R; blue - DAPI. (B) Fluorescence signal of S1R was quantified as the total cell fluorescence. (C) S1R gene expression was expressed as –ΔΔCt values. ***p-value < 0.001.**

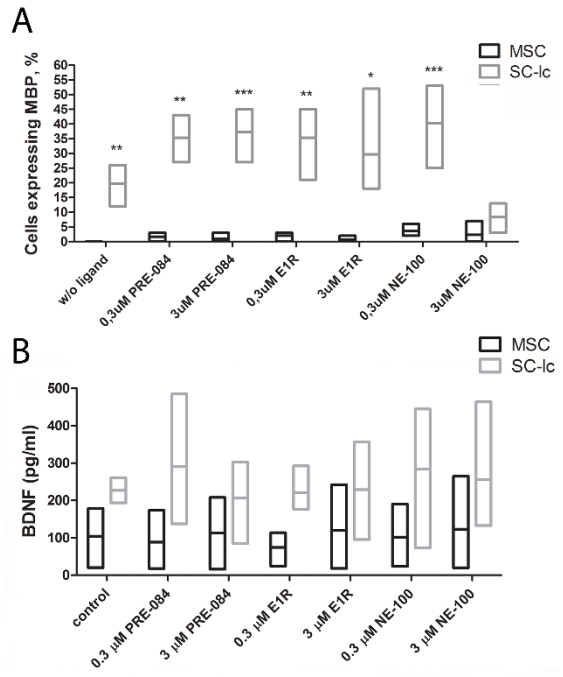


Fig. 8. **The impact of S1R ligands (0.3 and 3 µM) on the expression of MBP and secretion of BDNF in MSCs and SC-lcs. (A) Impact of S1R ligands on the expression of MBP in MSCs and SC-lcs (n = 3). The statistics indicate the comparison between MSCs and their respective SC-lcs. (B) Average BDNF secretion in three independent donor cell lines (n = 3). *p-value < 0.05, **p-value < 0.01, ***p-value < 0.001.**

### 3.2. Nanoparticle delivery to breast cancer cells by nanoengineered mesenchymal stem cells

#### 3.2.1. QD655 biocompatibility with mesenchymal stem cells

Due to MSC migratory properties, they could be used as drug delivery vectors to tumors. To test this hypothesis, we investigated MSC interaction with QDs.

To test if QD655 influence skin MSC phenotype and function, the release of QDs, Ki67 mesenchymal marker expression and trilineage differentiation was analyzed. The concentration-dependent cytotoxicity of QDs was analyzed in MSC cultures after 24 and 48 h in serum-containing medium and in a medium without serum. Viability was assessed using a colorimetric CCK-8 assay, which measures intracellular dehydrogenase activity.

Flow cytometry data revealed that MSCs incubated for 6 h in serum-free conditions accumulated more QDs compared with cells incubated in complete medium. QD-loaded MSCs we named nanoengineered MSCs. At a QD concentration of 2 nM, 100% of the cells were labelled with QDs in serum-free medium, whereas a 100% positive cell population was achieved after incubation with 16 nM QDs in complete medium (Fig. 9, A). Fluorescence intensity analysis revealed that the QDs accumulated in the cells in a concentration-dependent manner. MSCs incubated with QDs diluted in the serum-free medium accumulated 100-fold more QDs compared with the complete medium (Fig. 9, B). Under serum-free conditions, QD uptake saturation was achieved at 16 nM, whereas no saturation was achieved in cells incubated with QDs in complete medium even at a concentration of 32 nM (Fig. 9, B). Next, we analyzed the MSC viability in response to intracellular QD accumulation. Incubation time points were selected at 24 and 48 h to identify the QD-induced cytotoxic effects. We did not observe any cytotoxic effect on MSC viability when the QDs were applied in complete medium (Fig. 9, C). On the contrary, due to the 100-fold increase in the QD accumulation ratio under serum-free conditions, the toxicity of 30 and 50% was observed after 24 h of MCS incubation with 32 nM and 64 nM QD concentrations (Fig. 9, D). Interestingly, the cytotoxic effect was not observed after 48 h of incubation with QDs, which could be explained by the reduction of intracellular QD concentration due to cell division. Thus, we chose a QD concentration of 16 nM as optimal for the labelling of cells in complete medium, whereas 8 nM was optimal for cell labelling in serum-free medium for 6 h.

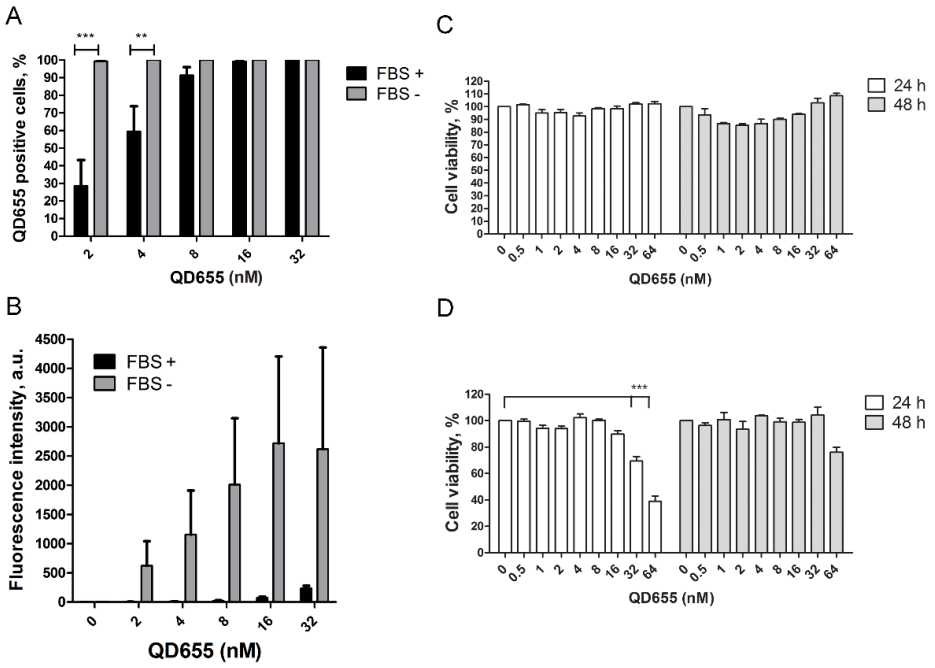


Fig. 9. **Characterization of the optimal QD655 incubation conditions in MSCs. QD655 uptake after 6 h of incubation of MSCs cultivated in complete (FBS +) or serum-free (FBS -) medium expressed as (A) the percentage of QD655-positive cells and (B) the QD655 accumulation intensity. The impact of QD655 on MSC viability after labelling in (C) complete and (D) serum-free medium following incubation for 24 h and 48 h. **p-value < 0.01, ***p-value < 0.001.**

After 6 h of MSC labelling with QDs (0 h in Fig. 10, A), the medium was changed to a fresh complete or serum-free medium and cells were incubated for 24 h and 48 h to check for QD signal. We observed a 30% decrease of the QD signal in cells propagated in complete medium and a 40% decrease of the QD signal under serum-free conditions after 24 h of incubation (Fig. 10). After 48 h, the number of QD-positive cells decreased even further in serum-free cultivated cells (Fig. 10, A). To determine whether MSCs release QDs in the environment after uptake, the supernatant was removed from cells after QD labelling. After rigorous rinsing, a fresh complete or serum-free medium was applied to the QD-labelled cells. Next, the QD fluorescence intensity was determined in cells at 24 and 48 h after labelling. Supernatant from primarily QD-labelled MSCs was transferred to fresh MSCs for secondary labelling experiments. After 24 h, 3% of the cells in complete medium had taken up QDs, whereas under serum-free conditions, 7% of MSCs had taken up QDs in the secondary labelling experiments (Fig. 10, B). After 48 h QD uptake was detectable in approximately 1.5% of cells cultivated either in complete or serum-free medium (Fig. 10, B). To exclude cell division as a QD signal reducing factor, we synchronized the MSC cell cycle by 24 h long serum starvation and then analyzed Ki67 expression after propagation in complete and

serum-free medium. MSCs, cultivated in serum-free medium, did not proliferate after 24 and 48 h, thereby excluding the probability of QD transfer to daughter cells, because QD signal loss occurs under serum-free conditions (Fig. 10, C).

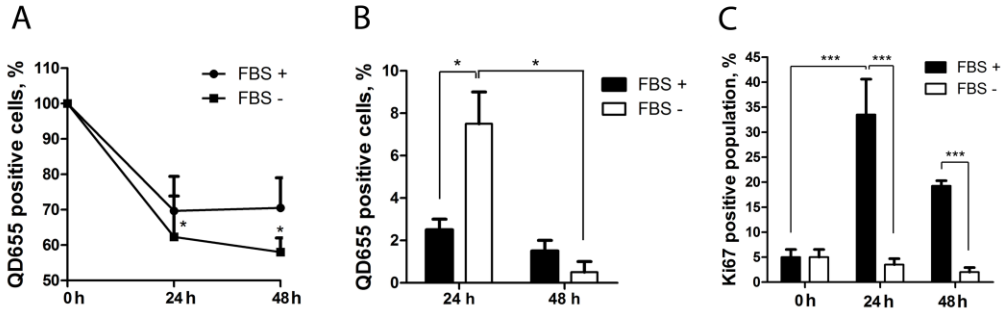


Fig. 10. **The release of QD655 from MSCs. (A) QD655 loss in complete medium (FBS +) and serum-free medium (FBS −) after 6 h of primary QD655 labelling (0 h), 24 h and 48 h after labelling. The statistical significance is shown in comparison to 0 h. (B) Secondary labelling experiment. Uptake of QDs in fresh MSCs labelled with supernatant from primarily labelled MSCs after 24 h incubation. (C) The comparison of Ki67 expression in complete and serum-free medium after labelling cell cycle synchronized MSCs (0 h) and after 24 h and 48 h of cultivation; *p-value < 0.05, ***p-value < 0.001.**

Mesenchymal marker CD90, CD73, hematopoietic marker CD34, CD45 and proliferation marker Ki67 expression in MSCs after QD labelling was not changed (Fig. 10-11). MSC trilineage differentiation into adipocytes, osteocytes and chondrocytes was not changed after QD loading (Fig. 12-13).

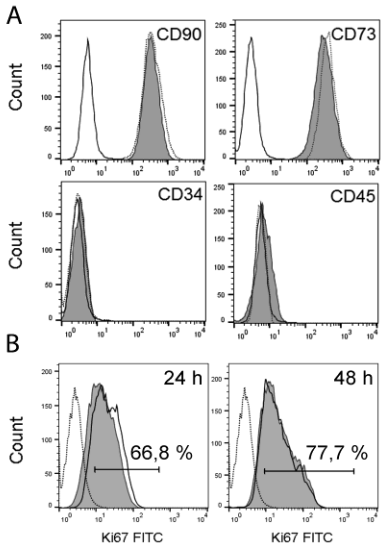


Fig. 11. **Representative data on the impact of QD655 on immunophenotype and proliferation of MSCs. (A) Characterization of MSC markers CD90, CD73 and hematopoietic markers CD34 and CD45 in MSCs. Open histogram: unlabeled cells, dotted-line histogram: MSCs without QD655, grey histogram: QD655-labelled**

**MSCs. (B) Ki67 expression in MSCs after 24 h and 48 h of incubation with 16 nM QD655. Open histogram: unlabeled cells, dotted-line histogram: isotype control, grey histogram: QD655-labelled cells.**

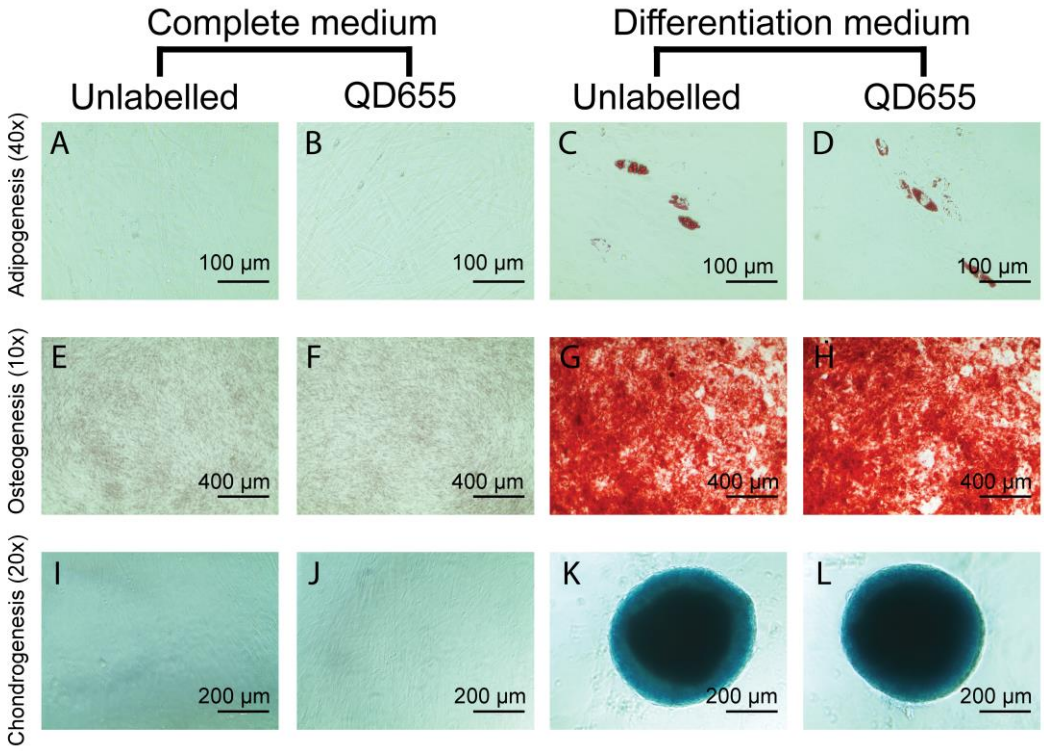


Fig. 12. **Differentiation of MSCs into adipocytes, chondrocytes and osteocytes. Oil Red O staining of cells in complete medium (A) without or (B) with QD655 labelling; cells in adipogenesis medium (C) without or (D) with QD655 labelling. (E, F) Alizarin Red S staining in cells in complete medium in the absence or presence of QD655; (G, H) cells in osteogenesis differentiation medium in the absence or presence of QD655. medium (I, J) Alcian Blue staining on cells in complete and (K, L) chondrogenesis differentiation medium in the absence or presence of QD655.**

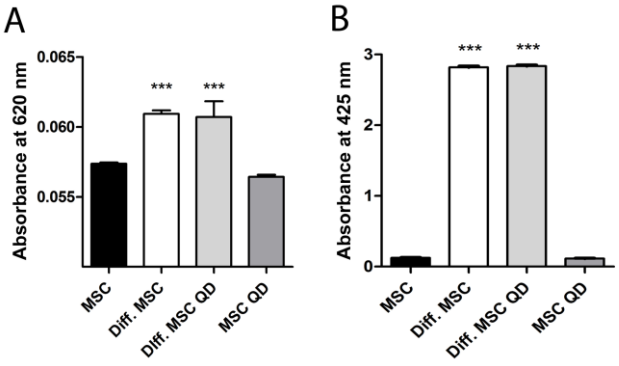


Fig. 13. **Quantification of osteogenesis and chondrogenesis in MSCs. (A) Absorbance of Alizarin Red S and (B) Alcian Blue solutions extracted from differentiated MSCs. Diff. MSC: differentiated MSCs, diff. MSC QD655: differentiated MSCs labelled with QD655. Significance compared between differentiated and undifferentiated samples; ***p-value < 0.001.**

### 3.2.2. QD655 endocytosis pathway in mesenchymal stem cells

To test the QD uptake route in MSCs, endocytic pathway analysis was performed. The effect of serum proteins on the efficiency of QD uptake was analyzed based on the comparison of QD uptake in complete and serum-free media (Fig. 14). The effect of endocytosis inhibitors differed between a complete and serum-free medium. In complete medium, a tendency of decreased QD uptake was observed using CPZ, an inhibitor of clathrin-mediated endocytosis (Fig. 14). In a serum-free medium, QD uptake was significantly inhibited by CPZ and nystatin, an inhibitor of caveolin/lipid raft-mediated endocytosis ($p < 0.01$) (Fig. 14, B, D). In serum-free medium, cells internalized more QDs according to the fluorescence intensity analysis (Fig. 14, C, D).

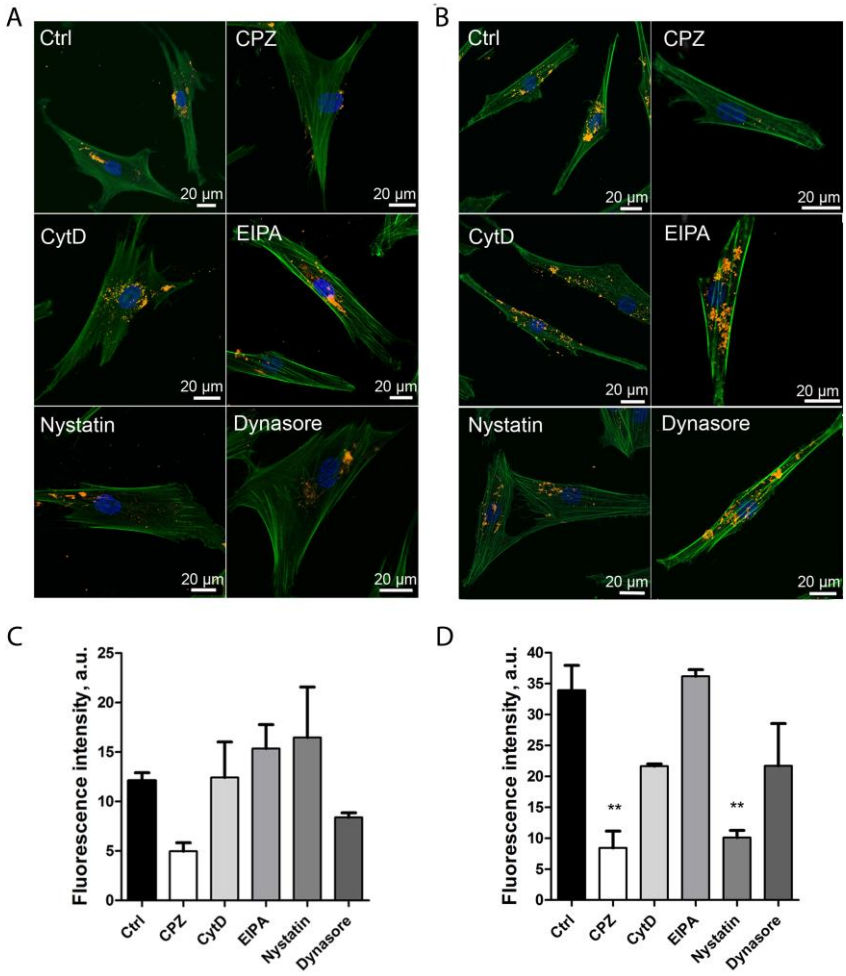


Fig. 14. **QD655 endocytic pathway in MSCs. QD655 uptake pathway in MSCs labelled with QD655 in (A) complete medium or in (B) serum-free medium. Uptake pathways were blocked using the endocytosis inhibitors CPZ, CytD, EIPA, nystatin and dynasore. Three overlaid channels represent Hoechst (blue), Phalloidin Alexa Fluor488 (green), carboxyl QD655 (yellow). Representative data are shown. QD655 fluorescence signal was quantified in (C) complete and (D) in serum-free medium cultivated MSCs. Statistical significance shown for the respective sample in comparison to control (Ctrl) sample; **p-value < 0.01.**

### 3.2.3. Mesenchymal stem cell and breast cancer cell three-dimensional culture model

To mimic cell-cell interactions *in vivo*, we developed a 3D co-culture using polyHEMA-coated plates. MSC aggregation was observed 3–6 h after seeding on polyHEMA-coated plates. 24 h later, cells formed compact and dense floating spheroids of 100 μm in diameter (Fig. 15, A, B). The diameter of the spheroids further increased after 48 and 72 h (Fig. 15, A, B). CD90 was used as a selective marker for MSCs because it is not expressed in MCF7 and MDA-MB-231 cells (Lobba et al. 2012). To ensure the stability of the selective marker, the expression of CD90 in 3D MSC culture was monitored over time. After 24 h in spheroid culture, 97% of MSCs remained CD90 positive. However, after 48, 72 and 96 h propagation on polyHEMA coating, CD90 expression was reduced to 92%, 81% and 88%, respectively (Fig. 15, C). Therefore, we chose 24 h as the optimal incubation time for 3D cell co-culture experiments to ensure the selectivity of the CD90 marker towards MSCs.

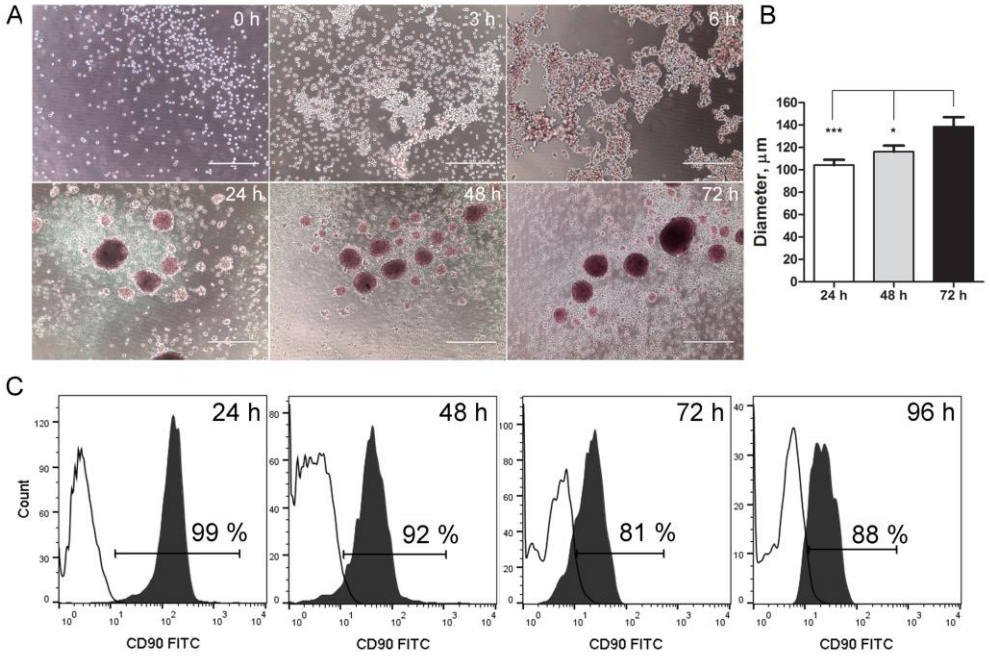


Fig. 15. **Characterization of MSCs in 3D culture conditions. (A) MSC spheroid formation on polyHEMA coating. Scale bar – 400 μm. (B) The change in the diameter of MSC spheroids in 3D culture over time. (C) The dynamics of CD90 expression in 3D cultivated MSCs. *$p$-value < 0.05, ***$p$-value < 0.001.**

Next, we sought to determine the stability of the QD signal in MSC spheroids. QD release was estimated in MSCs that were labelled with QDs in complete or serum-free medium in two dimensional (2D) culture and seeded on polyHEMA coatings to form spheroids. After 24 h, only 56% of MSCs that were labelled with QDs in complete medium and formed 3D structures had

retained the QD signal. Following 48 and 72 h of incubation, the number of QD-labelled MSCs in 3D culture decreased further to 33% and 35%, respectively (Fig. 16, A). The rapid reduction in the QD signal after 24 h was confirmed by fluorescence intensity analysis (Fig. 16, B). On the contrary, 100% of MSCs that were labelled in serum-free conditions remained QD positive until 72 h of incubation (Fig. 16, C). Despite the fact that 100% of the MSC population was QD positive in serum-free medium until 72 h, we observed a 5.5-fold/5-fold decrease in the fluorescence intensity, respectively, indicating that QD elimination occurs (Fig. 16, D). As mentioned previously, a significantly increased intracellular accumulation of QDs was observed in serum-free medium (Fig. 16, A, B), and the QD elimination effect was subsequently more pronounced (Fig. 16, D). Thus, we chose to label MSCs with QDs in serum-free medium to ensure the highest load of intracellular QDs for further 3D co-culture experiments.

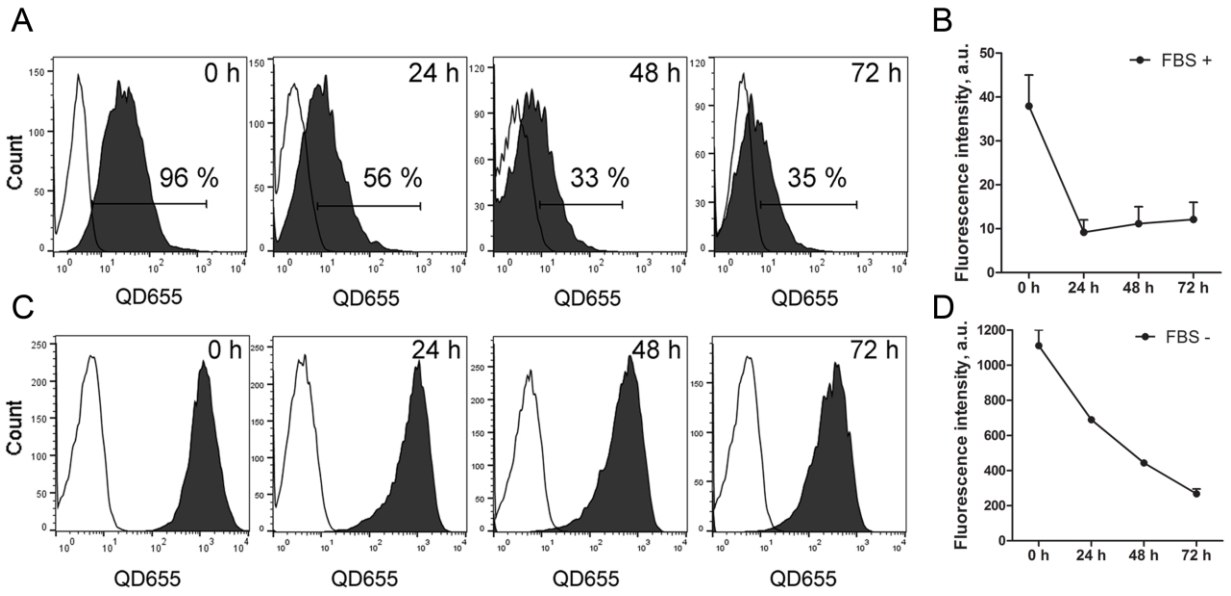


Fig. 16. **The dynamics of QD655 signal in MSC 3D culture. Representative data of MSC QD655 signal analysis in 3D culture after labelling in (A) complete (FBS +) or (C) serum-free (FBS -) medium. The changes of the QD655 fluorescence signal intensity in the 3D MSC population after labelling in (B) complete and in (D) serum-free medium.**

MCF7 and MDA-MB-231 cells formed loose, floating aggregates in 3D culture conditions (Fig. 17, A). MCF7 and MDA-MB- 231 cells were labelled with 8 nM QDs in 2D and 3D culture to evaluate the differences in uptake efficiency under both conditions. We observed that MCF7 cells exhibited increased QD internalization efficiency in standard culture conditions (2D) compared with 3D culture ($p < 0.05$) (Fig. 17, B). To the contrary, MDA-MB-231 internalized 6-

fold more QDs in 3D culture compared with 2D ($p < 0.001$) (Fig. 17, B). Such discrepancy in uptake efficacy might be associated with different endocytosis pathways. MCF7 cells internalized QDs through phagocytosis and clathrin/caveolae-dependent endocytosis, whereas the clathrin/caveolae-dependent pathway dominated in MDA-MB-231 cells in monocultures (data not shown).

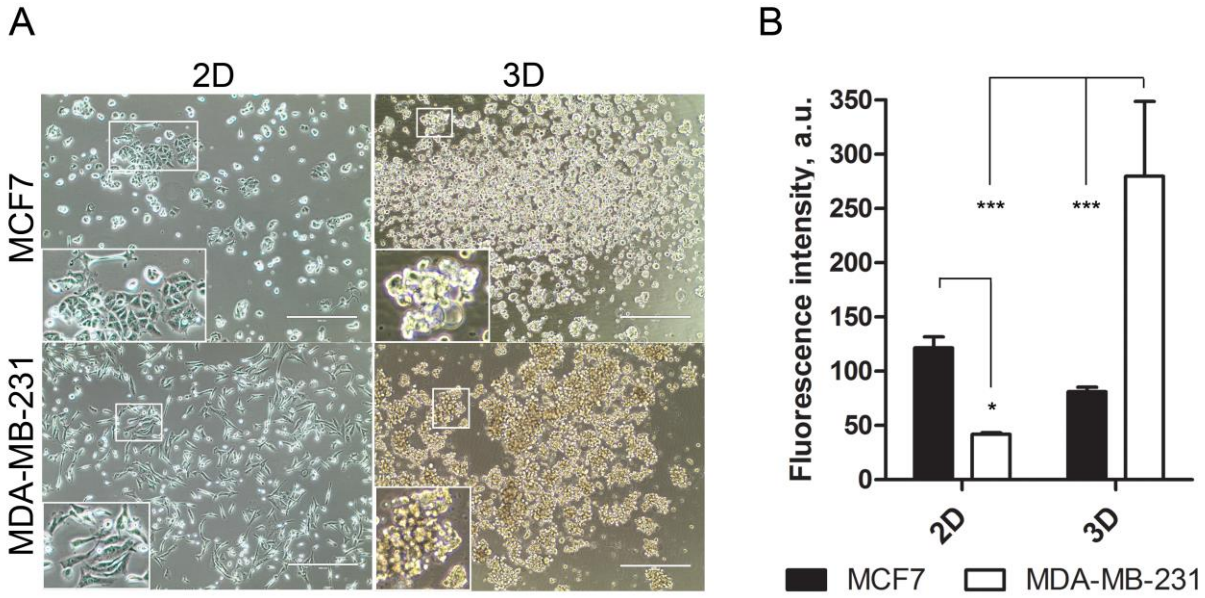


Fig. 17. **Comparison of MCF7 and MDA-MB-231 properties in 2D and 3D culture conditions. (A) The morphology of MCF7 and MDA-MB-231 cells in 2D and 3D culture. Scale bar – 400 µm. (B) QD655 uptake efficiency in MCF7 and MDA-MB-231 cells in 2D and 3D culture expressed as the intracellular QD655 fluorescence intensity. *$p$-value < 0.05, ***$p$-value < 0.001.**

Cells in a 3D culture formed floating and dense spheroids. Therefore, we sought to analyze the effect of the 3D culture conditions on cell viability using CCK8 assay (Fig. 18). MSC and breast cancer cell populations were distinguished by CD90 expression, thus allowing viability estimations in each cell type separately. Cell viability in 2D culture was greater than 95% (data not shown). MSCs cultivated in 3D monocultures were fully viable after 24 h; nevertheless, a distinct decrease in viability of 26% was observed after 48 h (Fig. 18, A). MCF7 and MDA-MB-231 cell viability was not changed after 24 h. However, after 48 h, the viability of MCF7 cells was reduced by 31% (Fig. 18, A). The viability of MDA-MB-231 cells remained unchanged after 24 h and 48 h in 3D culture (Fig. 18, A). In 3D co-culture, MSC/MCF7 viability after 24 h decreased by 9%, of which 2% accounted for MSCs and 7% for MCF7. In MSC/MDA-MB-231 co-culture, 11% of cells were dead, of which 6% were MSCs and 5% were MDA-MB-231 after 24 h of cultivation. The cell

survival rate in co-culture decreased after 48 h of propagation. The viability of cells in MSC/MCF7 co-culture decreased by 23% (10% MSCs and 13% MCF7), whereas the number of dead cells was 13% (6% MSCs and 7% MDA-MB-231) in MSC/MDA-MB-231 co-culture after 48 h. Viability was considered as another reason to select the 24 h incubation in 3D co-culture as the optimal time point for the study.

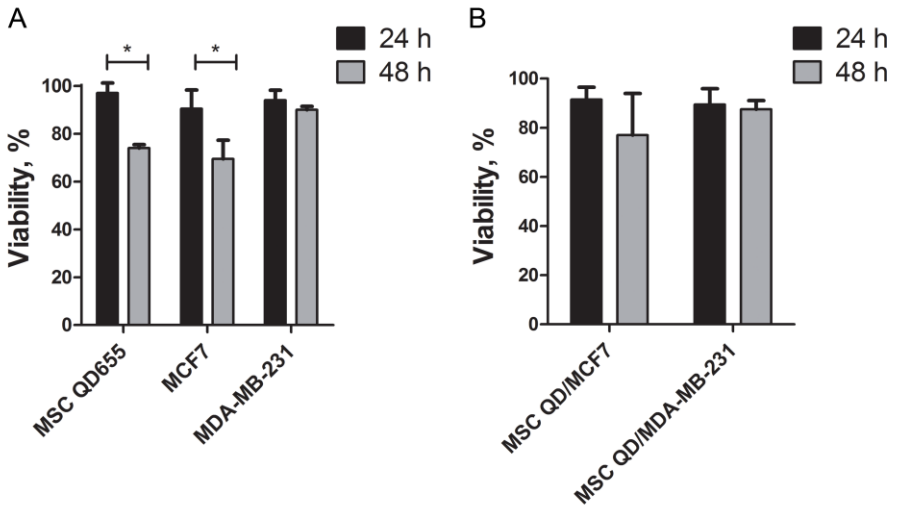


Fig. 18. **The viability of MSCs, MCF7 and MDA-MB-231 cells in spheroids. The viability of cells was analyzed in (A) 3D monocultures and (B) 3D co-cultures after 24 h and 48 h of cultivation on PolyHEMA coatings. *$p$-value < 0.05.**

### 3.2.4. QD655 transfer from nanoengineered mesenchymal stem cells to breast cancer cells in a three-dimensional co-culture model

QD-labelled cells were named nanoengineered MSCs. The foremost aim of our study was to obtain experimental proof that nanoengineered MSCs could convey QDs to the cancer cells in 3D co-culture conditions (Fig. 19). Indeed, our data clearly demonstrate that after 24 h in 3D co-culture, 18% of MCF7 cells (Fig. 19, F) and 31% of MDA-MB-231 cells (Fig. 19, G) had internalized QDs as noted by the appearance of single QD label-positive cells in the lower right quadrant of the dot plot. Importantly, 96% of the QD-loaded MSC population was CD90 positive in 3D monoculture (Fig. 19, C). As expected, MCF7 (Fig. 19, D) and MDA-MB-231 cells (Fig. 19, E) were CD90 negative in 3D monocultures. The proof of principle was demonstrated also using EpCAM positive MCF cells. Similarly, to the previous data obtained with CD90 as a selective marker in the co-culture model (Fig. 19), the QD transfer efficiency from nanoengineered MSCs to EpCAM positive MCF7 cells was on average 18% (Fig. 20). The QD transfer from MSCs to cancer cells was also visualized by fluorescence imaging where CD90-negative/QD-positive

cells represented cancer cells that have taken up the QDs released from MSCs during 3D co-culture (Fig. 21).

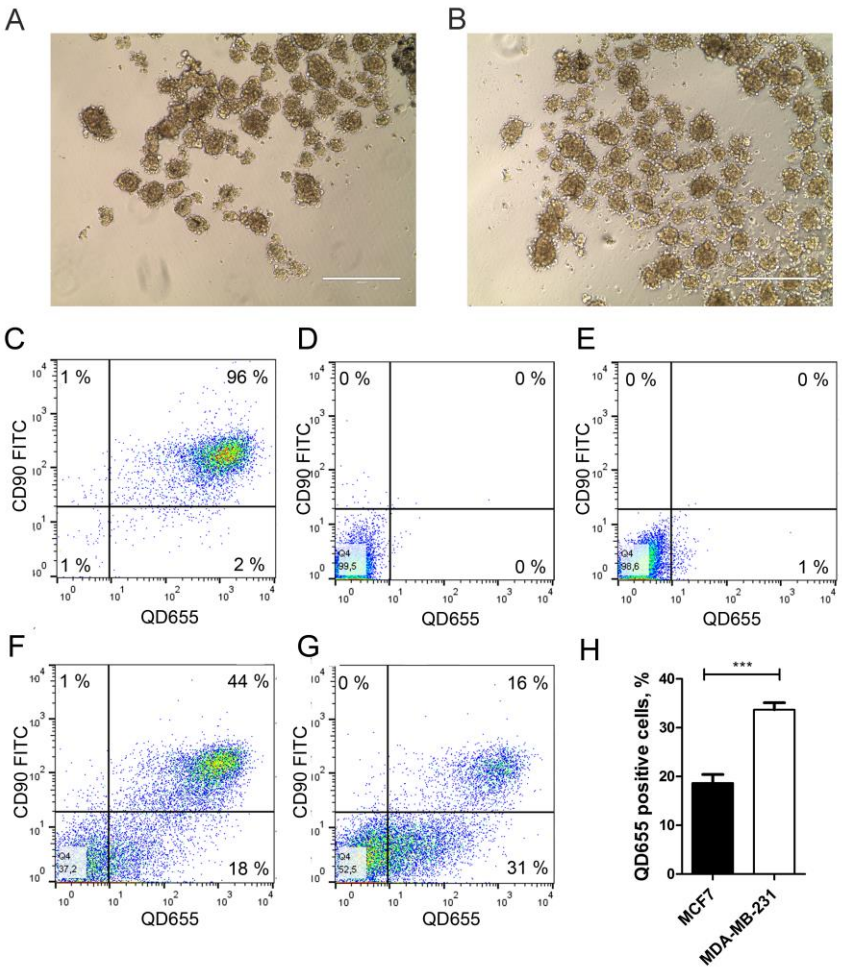


Fig. 19. **QD655 uptake in MCF7 and MDA-MB-231 cells in 3D co-culture. (A) Morphology of nanoengineered MSC/MCF7 and (B) nanoengineered MSC/MDA-MB-231 spheroids after 24 h of co-culture. Scale bar – 400 µm. (C) Nanoengineered MSCs, (D) MCF7 and (E) MDA-MB-231 cells were stained with CD90 to distinguish MSCs and cancer cell populations. Lower right quadrant in the dot plot shows the single QD655 positive population (QD labelled cancer cells) in (F) nanoengineered MSC/MCF7 and (G) nanoengineered MSC/MDA-MB-231 3D co-cultures. Representative data shown. (H) QD655 transfer efficiency from MSCs to cancer cells illustrated by the percentage of QD655-positive/CD90-negative cells (*n* = 3). ****p*-value < 0.001.**

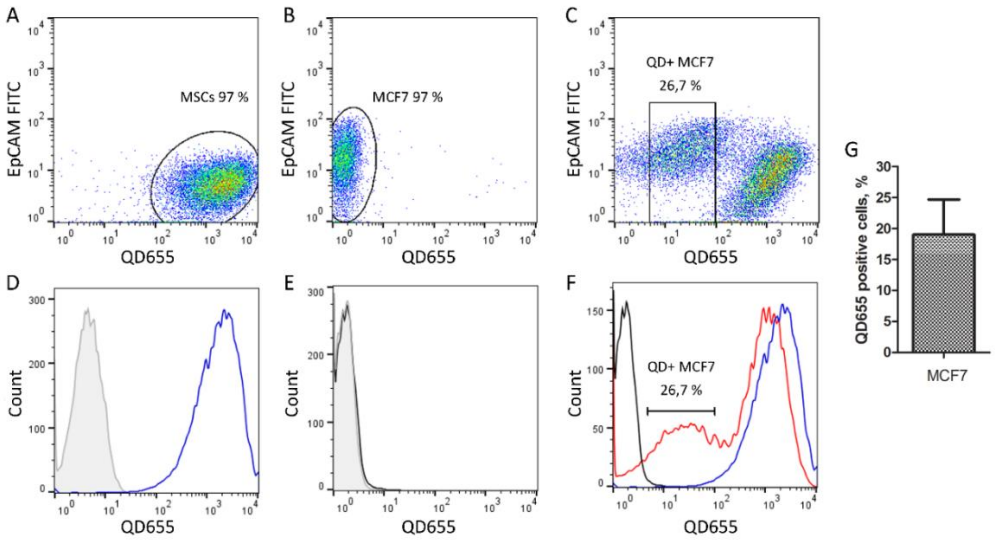


Fig. 20. **QD655 transfer from nanoengineered MSCs to MCF7 cells using EpCAM as a selective marker for MCF7 cells. Co-culture populations were separated by marker expression and QD655 fluorescence. (A) Nanoengineered MSCs labelled with QD655. (B) MCF7 cells stained with EpCAM antibody. (C) Nano-engineered MSCs and MCF7 cells in a 3D co-culture. Square represents QD positive MCF7 cells. (D) QD655 loaded MSCs. Grey histogram – negative control, blue histogram – QD655 loaded MSCs. (E) QD655 signal in QD655 unlabeled MCF7 cells. (F) Nano-engineered MSC and MCF7 co-culture (red histogram) overlayed with QD655 negative MCF7 sample (black histogram) and nanoengineered MSC sample (blue histogram) (representative sample shown). (G) QD655 transfer efficiency from nanoengineered MSCs to MCF7 cells after 24 h of 3D co-culture (n = 3). On average 18% of MCF7 cells uptake QD655 from nanoengineered MSCs (n = 3).**

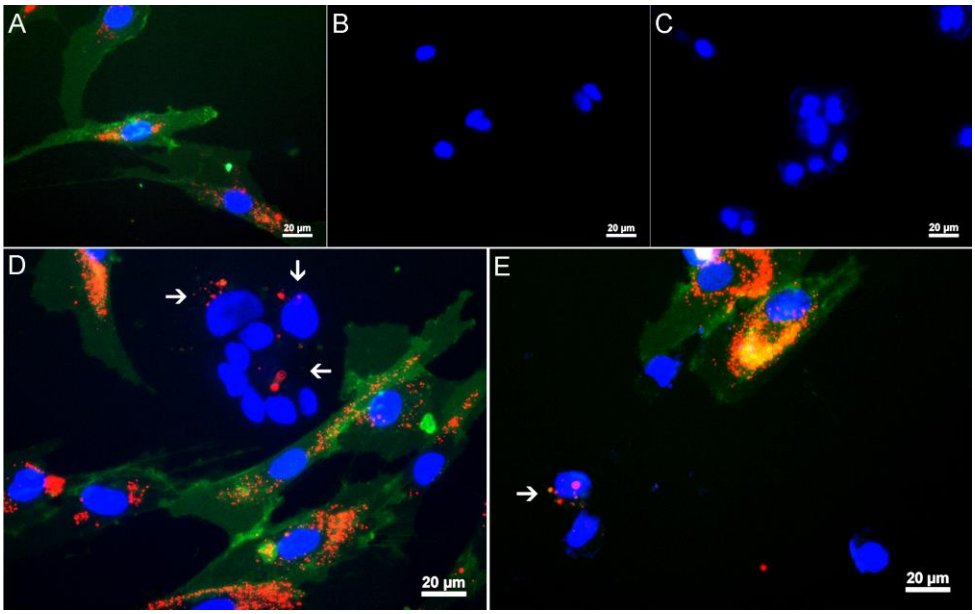


Fig. 21. **Fluorescence imaging of QD655 intracellular accumulation in MCF7 and MDA-MB-231 cells during 3D co-culture. (A) Nanoengineered MSCs, (B) MCF7 and (C) MDA-MB-231 cells were stained with**

**CD90 FITC to distinguish cell populations. Single QD655-positive/CD90-negative cells observed in nanoengineered (D) MSC/MCF7 and (E) nanoengineered MSC/MDA-MB-231 co-cultures. White arrows indicate cancer cells with internalized QD655. Blue – Hoechst, green – CD90 FITC, red – QD655. Scale bar – 20 μm.**

### 3.3. Impact of anthocyanidins on mesenchymal stem cell trilineage differentiation

MSC trilineage differentiation model can be used to screen pharmacologically active compound effects on adipogenesis, osteogenesis and chondrogenesis *in vitro*. Up to date no one has analyzed how plant derived pigment molecules anthocyanidins affect MSC trilineage differentiation. Three anthocyanidins were selected for the study – malvidin, cyanidin and delphinidin.

Anthocyanidin cytotoxicity on MSCs was tested in the concentration range of 25 to 200 μM following 24, 48 and 72 h incubation periods. All anthocyanidins induced concentration-dependent cytotoxicity (Fig. 22, A-C). The highest cytotoxicity for all compounds was observed at 200 μM, when MSC viability decreased to 50%–70% in malvidin-, to 40%–50% in cyanidin- and 30% in delphinidin-treated samples (Fig. 22, A, B, C, respectively). Slight variability in cytotoxicity was observed depending on the incubation time at concentrations above 50 μM for malvidin and at concentrations from 25 to 100 μM for cyanidin. The delphinidin concentration-dependent cytotoxicity was comparable at all time-points tested. Based on the cytotoxicity data, the anthocyanidin concentration of 25 μM was selected for further experiments. The concentrations of 10 and 100 nM diabetes *mellitus* and anti-obesity drug liraglutide were selected according to the data published in the literature (Chen et al. 2017).

MSC differentiation into adipocytes was confirmed by the Oil Red O stain for lipid accumulation (Fig. 23, A). Intracellular accumulation of lipids was present in all differentiated samples. Neither anthocyanidins nor liraglutide visually decreased the lipid accumulation in cells compared with the untreated MSCs (positive control). To quantitatively assess the impact of anthocyanidins and liraglutide on adipogenesis, we analyzed the expression of three adipose tissue-related genes, *FABP4*, *LPL* and *Adiponectin* using real-time RT-PCR (Fig. 23, B–F). Anthocyanidins exerted diverse effects on adipose tissue-related gene expression in adipogenesis samples. 25 μM malvidin and cyanidin significantly increased the expression of *Adiponectin*, *FABP4* and *LPL* on average 1.5-2-fold ($p < 0.05$ – $p < 0.001$) (Fig. 23, B-C). Remarkably, 25 μM delphinidin showed an inhibitory effect on adipogenesis, similarly to the antidiabetes and antiobesity drug liraglutide. Delphinidin downregulated the expression of *FABP4* and *Adiponectin*

(Fig. 23, D), while liraglutide downregulated *Adiponectin* (10 nM, 100 nM) and *FABP4* (10 nM) expression ($p < 0.05/p < 0.01$) (Fig. 10, E- F).

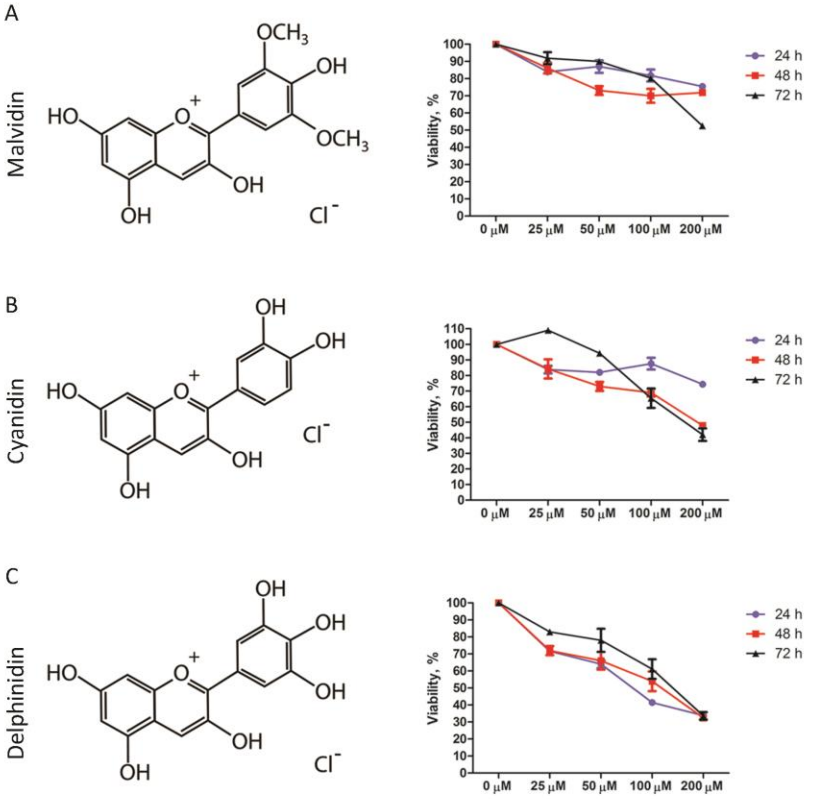


Fig. 22. **Effects of anthocyanidins on MSC viability. Chemical structures of (A) malvidin, (B) cyanidin and (C) delphinidin, and concentration-dependent effects on MSC viability after treatment for 24, 48 and 72 h.**

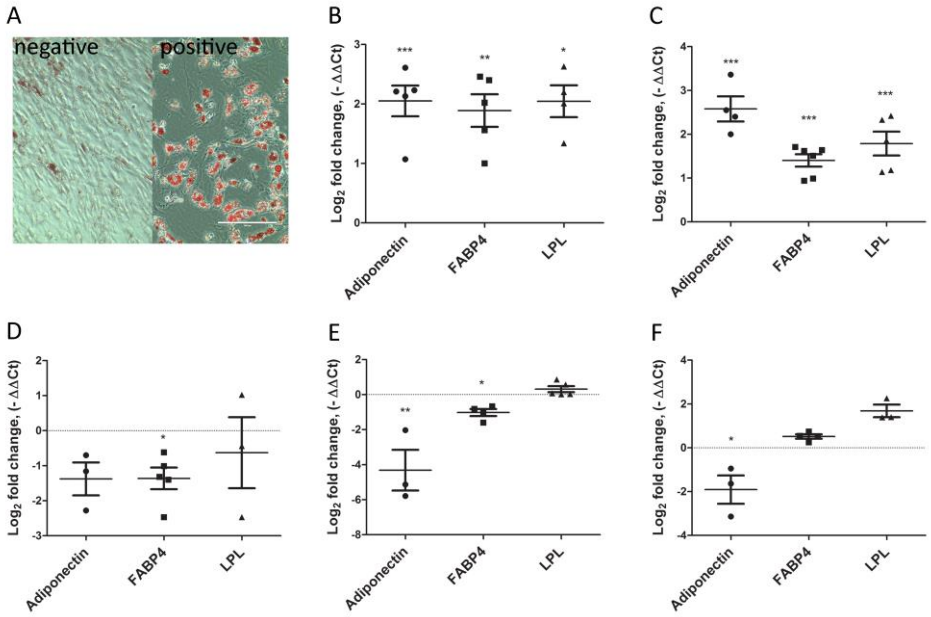


Fig. 23**. Effects of anthocyanidins on MSC differentiation into adipocytes. (A) Oil Red O staining for lipid accumulation in undifferentiated (negative) and differentiated MSCs (positive) (representative sample). Scale**

**bar – 200 µm. Adipocyte specific gene expression in (B) malvidin-, (C) cyanidin-, (D) delphinidin-, (E) 10 nM lliraglutide-, (F) 100 nM liraglutide-treated MSCs after adipogenic differentiation (n ≥ 3). Gene expression in anthocyanidin and liraglutide-treated cells was compared to the base-line expression level in anthocyanidin or liraglutide-untreated cells. Liraglutide was used as a reference drug. *p-value < 0.05, **p-value < 0.01, ***p-value< 0.001.**

After differentiation into osteocytes, MSCs were stained with Alizarin Red to assess the accumulation of calcium deposits. Compared to the non-differentiated cells, all differentiated cell samples exhibited calcium accumulation, as shown by the Alizarin Red staining (Fig. 24, A). However, the quantification of the Alizarin Red stain revealed that cells treated with 25 µM malvidin exhibited significantly increased calcium accumulation in osteocytes, while cells treated with 25 µM cyanidin, delphinidin and 10–100 nM liraglutide exhibited decreased calcium deposits compared to the positive control cells (Fig. 24, G). To analyze the effects of anthocyanidins and liraglutide, we tested the expression of five osteocyte-related genes *ALPL, Col1a1, Osteocalcin, Runx2* and *BMP-2* by real-time RT-PCR (Fig. 24, B–F). Similar to cytochemical staining, gene expression analysis revealed that malvidin upregulates *Runx2* ($p < 0.05$) and *BMP-2* ($p<0.01$) expression while cyanidin and delphinidin did not change adipocyte gene expression levels comparing to untreated cells (Fig. 11, B-D). Interestingly, the anti-diabetes drug liraglutide significantly upregulated *BMP-2* ($p < 0.001$) and downregulated *Col1a1* ($p < 0.001$) expression (10 nM), whereas *Osteocalcin* expression was upregulated by the treatment of liraglutide (100 nM) ($p < 0.01$). BMP-2 secretion correlated with the gene expression data, which confirmed that malvidin and liraglutide promoted BMP-2 secretion and altogether facilitated MSCs osteogenesis (Fig. 24, H).

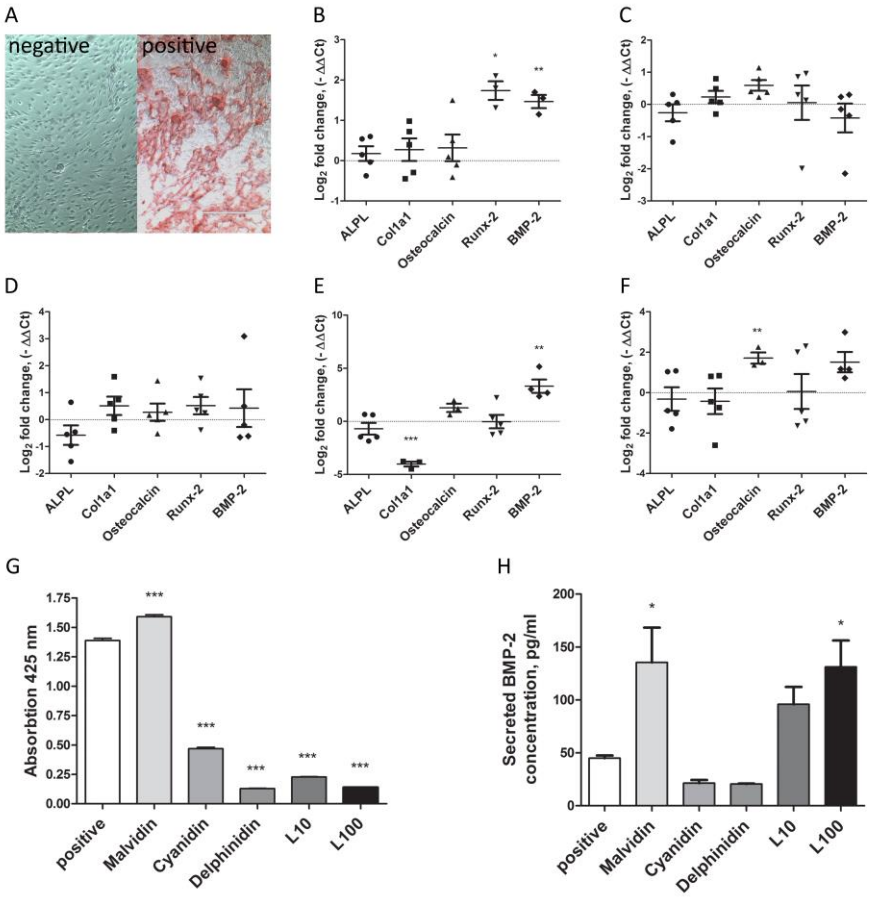


Fig. 24. **Effects of anthocyanidins on MSC differentiation into osteocytes. (A) Alizarin Red S staining for calcium deposits in undifferentiated (negative) and differentiated MSCs (positive) (representative sample). Scale bar – 400 µm. Osteocyte specific gene expression in (B) malvidin-, (C) cyanidin-, (D) delphinidin-, (E) 10 nM liraglutide-, (F) 100 nM liraglutide-treated MSCs after osteogenic differentiation (n ≥ 3). (G) Spectroscopic quantification of Alizarin Red stain at 425 nm. (H) BMP-2 secretion analysis in MSCs after osteogenic differentiation (n ≥ 3). Expression in anthocyanidin and liraglutide-treated cells was compared to the base-line expression level of anthocyanidin or liraglutide-untreated cells. Liraglutide was used as a reference drug. *p-value < 0.05, **p-value < 0.01, ***p-value < 0.001.**

MSCs during chondrogenesis formed the characteristic spheroidal structures. After differentiation, chondrocyte spheroids were stained with Alcian Blue dye for glycosaminoglycan detection (Fig. 25, A). Quantification of the stain from the spheroids revealed that delphinidin promoted glycosaminoglycan content in MSCs after chondrogenic differentiation compared to the control ($p < 0.001$) (Fig. 25, G). Three articular chondrocyte markers *Sox9, Col2a1* and *Aggrecan* were selected for gene expression analysis. *Runx2* and *BMP-2* served as hypertrophic chondrocyte markers (Fig. 25, B–F). Gene expression analysis revealed that cells treated with 25 µM cyanidin and delphinidin exhibited a significant 1.5–2-fold increase in chondrocyte structural gene *Col2a1*

and *Aggrecan* expression compared to the untreated positive control cells ($p < 0.01$ /$p < 0.001$) (Fig. 25, C–D). Neither *Sox9* nor hypertrophic chondrocyte marker *Runx2* and *BMP-2* expression in MSCs was influenced by anthocyanidin treatment. Additionally, BMP-2 secretion was analyzed (Fig. 25, H). Although higher BMP-2 secretion was observed in anthocyanidin-treated samples than in the untreated control sample, the difference was not statistically significant.

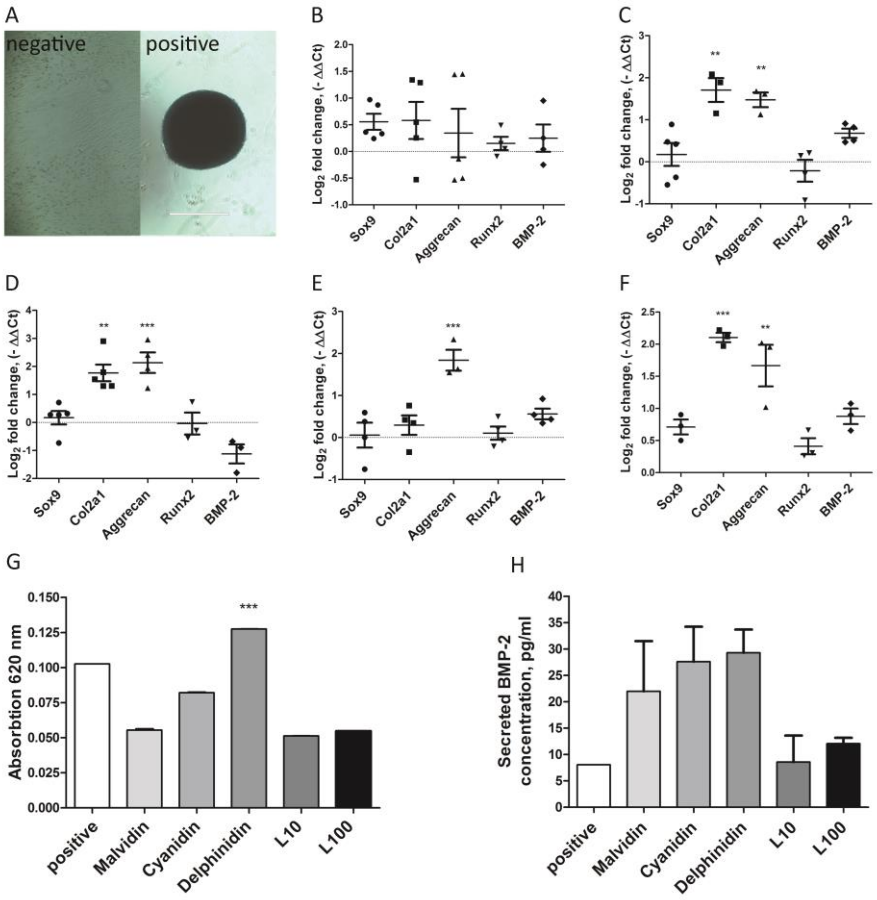


Fig. 25. **Effects of anthocyanidins on MSC differentiation into chondrocytes. (A) Alcian Blue staining of spheroids for glycosaminoglycans in undifferentiated MSCs (negative) and differentiated MSCs (positive) (representative sample). Scale bar – 400 µm. Chondrocyte specific gene expression in (B) malvidin-, (C) cyanidin-, (D) delphinidin-, (E) 10 nM liraglutide-, (F) 100 nM liraglutide-treated MSCs after chondrogenic differentiation ($n \geq 3$). (G) Spectroscopic quantification of the Alcian Blue stain at 620 nm in MSCs after chondrogenic differentiation. (H) BMP-2 secretion analysis in MSCs after chondrogenic differentiation ($n \geq 3$). Expression in anthocyanidin and liraglutide-treated cells were compared to the baseline expression level of anthocyanidin or liraglutide-untreated cells. Liraglutide was used as a reference drug. *p-value < 0.05, **p-value < 0.01, ***p-value < 0.001.**

# 4. DISCUSSION

## 4.1.Mesenchymal stem cell differentiation into Schwann cells

Previous studies have confirmed that adipose, skin, dental pulp and periodontal ligament derived MSCs in an undifferentiated state are highly positive for the early neuronal marker tubulin-βIII and for the late neuronal marker NeuN, while only 30% of the culture were positive for neural progenitor marker nestin (Foudah et al. 2014). An early study made by our group has demonstrated that skin-derived MSCs are highly nestin positive while in bone marrow, heart and adipose tissue-derived MSCs had a lower nestin expression (Riekstina et al. 2009). We now tested a broad panel of neuroectodermal markers to characterize skin MSC phenotype. It was demonstrated that MSCs express neural markers *Nestin, Tubulin-βIII,* glial markers *Sox10, GFAP* and neural crest lineage markers *p75NTR, Notch1, Integrin-α4, ErbB3, Ap2α* and *Jun-c* in an undifferentiated state (Fig. 4, A) indicating that skin MSC population contains a subpopulation of NCSC-like cells as reported elsewhere (Biernaskie et al. 2006). This observation encouraged us to test MSC ability to differentiate towards a Schwann cell phenotype. The majority of protocols in the literature exploit neuregulin and forskolin for the Schwann cell phenotype induction in MSCs (Biernaskie et al. 2006, Wakao et al. 2010) and similarly did we. After eight-day long differentiation we observed a SC-lc morphology which is characterized by an elongated, bipolar cell shape (Wakao et al. 2010). Further characterization of SC-lcs revealed an upregulated S100b expression (Fig. 5, D) which is associated with myelinated Schwann cell phenotype (Mata et al. 1990). This statement is complemented by a significant upregulation of myelin marker *MBP* (Fig. 5, E). Together with the increase in S100b and *MBP*, we observed a decreased expression of *p75NTR* and *Integrin-α4* (Fig. 5, E) which propose the shift from NCSC phenotype towards a specialized myelinating Schwann cell phenotype. Myelinating Schwann cell phenotype is characterized by an expression of Sox10, S100b, Krox20, Oct6, MBP and myelin protein zero (MPZ) (Liu et al. 2015). In PNS BDNF is secreted by motor neurons, dorsal root ganglion neurons and Schwann cells. BDNF promotes axon regeneration after a peripheral nerve injury and is known as a hallmark for repair Schwann cell phenotype (Jessen and Mirsky 2016, McGregor and English 2018). We have detected that MSCs synthesize BDNF in an undifferentiated state. Regardless, it was confirmed that BDNF production is significantly upregulated after differentiation into SC-lcs (Fig. 5, F). A high variation between donor MSCs was apparent, however analyzing the data separately, an increase was present in each donor SC-lcs indicating that skin MSC-derived SC-lcs could promote peripheral axon regeneration as already demonstrated by Cooney et al. (Cooney et al. 2016).

Next, we were interested to employ the established MSC glial differentiation protocol in pharmacologically active compound screening. In collaboration with prof. Maija Dambrova group at OSI, the role of S1R in MSC-derived SC-lcs was investigated. S1R is a multi-functional protein located at the endoplasmic reticulum membranes that are physically associated with the mitochondria (Hayashi 2015). Changes or dysfunction of S1R are associated with neurological disorders such as amyotrophic lateral sclerosis, Alzheimer's disease, Huntington's disease. The use of S1R ligands displays neuroprotective effects while a loss of S1R promotes neurodegenerative phenotypes (Ryskamp et al. 2019).

According to literature S1R is potentially involved in the differentiation of oligodendrocytes, regulation of myelination and lipid transport to the myelin membrane (Hayashi and Su 2004, Weng et al. 2017). It is known that S1R plays a role in pain mediation centrally and peripherally (Romero et al. 2012). The expression of S1R has been shown in Schwann cells, however, its role is not clearly defined (Palacios et al. 2004). This prompted us to look for S1R expression in SC-lcs. According to our data, S1R expression in SC-lcs was significantly increased compared to MSCs (Fig. 7). Therefore, three S1R ligands – S1R selective agonist PRE-084, S1R positive allosteric modulator E1R and selective antagonist NE-100 were used to elucidate the impact of S1R on Schwann cell differentiation. MBP and BDNF were selected as Schwann cell-specific markers for analysis. No significant change in the BDNF secretion could be observed in SC-lcs after S1R ligand treatment. Although results in each donor cell sample showed that the BDNF secretion has increased after differentiation, due to the high interpatient variability a general conclusion could not be made (Fig. 8, B). MBP analysis showed that the addition of S1R agonists PRE-084, positive allosteric modulator E1R at 0.3 and 3 μM concentrations and antagonist NE-100 at concentration 0.3 μM increased MBP expression in SC-lcs comparing to ligand untreated SC-lcs. Interestingly, antagonist NE-100 at 3 μM concentration inhibited MBP expression in SC-lcs, thus indicating towards a possibility that S1R blocking may result in a decreased myelination by Schwann cells (Fig. 8, A). This crucial finding indicates that S1R might play a role in the regulation of myelinating activity by Schwann cells.

To summarize, the expression of S1R is highly upregulated in SC-lcs in comparison to undifferentiated MSCs. S1R selective antagonist NE-100 inhibits the expression of MBP in SC-lcs. These results indicate that further studies would be necessary to investigate if S1R ligands could be used to regulate Schwann cell myelination after peripheral nerve injuries.

### 4.2. Nanoparticle delivery to tumor cells by nanoengineered mesenchymal stem cells

#### 4.2.1. Characterization of QD655 and mesenchymal stem cell interactions

It has been proposed that MSC migration towards tumor sites *in vivo* could be used to deliver diagnostic and therapeutic nano-agents. Studies on glioma (Wang et al. 2018), prostate cancer (Huang et al. 2019), breast cancer (Cao et al. 2018) and lung cancer (Zhao et al. 2017) models have confirmed the validity of this approach. Before the investigation of NPs, it is crucial to approve the biocompatibility with the vehicle cells. Among the wide variety of NPs investigated, QDs have perhaps the most extensive applications. QDs exhibit broad excitation and narrow photoluminescence emission spectra, size-dependent photoluminescence emission, brightness and high photostability which makes them promising candidates for cell-imaging and tumor-targeting (Zrazhevskiy and Gao 2013, Dapkute et al. 2017). It should be kept in mind though that there is a great deal of concern about the potential hazards of QDs due to the cadmium content in its core. The toxicity of QDs is therefore a topic of controversy. The potential toxicological effects of QDs are usually based on the release of free cadmium (Chen et al. 2011). However, QD shell and surface coatings protect the core, which contains semiconductor materials. Unless coating is damaged, QDs are mainly non-toxic (Walling et al. 2009).

QD655 were chosen for our targeted NP delivery model because of the emission maximum at 655 nm, narrow emission wavelength, very high photostability and bright fluorescence which make them suitable candidates for imaging. First, the biocompatibility of QD655 with skin-derived MSCs was tested. A different methodology was used to perform an extensive characterization of QD effects on MSC phenotype e.g. marker expression and differentiation ability. It was confirmed that MSC viability was not compromised by QD labelling up to 64 nM concentration (Fig. 9). No changes in proliferation marker Ki67 expression and mesenchymal stem cell marker expression profile, as well as trilineage differentiation were observed (Fig. 10-12), indicating that QDs are biocompatible and do not alter the properties of MSCs. Similar results have been reported in rat MSCs where QD labelling up to 50 µl/ml did not impair the viability, surface marker expression and multipotency of MSCs (Liu et al. 2015).

It was observed that QD signal is eliminated from MSCs over time (Fig. 10). The suggested mechanisms for the QD signal decrease over time are cell division, excretion and degradation (Pi et al. 2010, Oh and Park 2014). To exclude the possibility of a signal loss due to cell division, we performed MSC labelling in the medium without FBS supplement to mimic the cell cycle arrest. The lack of cell proliferation was confirmed by Ki67 expression (Fig. 10, C). It was noted that the

QD signal decreased despite the absence of FBS in cell culture medium, therefore we concluded that it was not caused by cell proliferation. Secondary labelling of fresh MSCs with the medium removed from QD-labelled MSCs was performed. QD uptake in MSCs was detected indicating that there is indeed a QD release in the medium from MSCs after primary labelling (Fig. 10, B). The fact that NPs are released from MSCs is highly important if one intends to use MSCs as NP delivery vectors. Secondary labelling efficiency was higher in the absence of FBS in the cell culture medium. This result indicates that the presence of FBS in cell culture medium induces a formation of protein corona around QDs which in turn could interfere with the NP uptake by target cells. The protein corona has been shown to affect the NP interaction with cells, cytotoxicity, membrane adhesions, uptake and transport (Abdelkhaliq et al. 2018). Altogether, we have demonstrated that MSCs release QDs in the cell culture supernatant and that could be as a result of membrane transporters that eliminate toxic reagents from the cells. Adenosine triphosphate-binding cassette transporters (ABC) possess a principal mechanism for the protection of stem cells (Dean 2009). ABC transporters have been shown to regulate the cellular accumulation and toxicity of QDs in human breast cancer cells SK-BR-3. Furthermore, smaller size QD accumulation in cells caused a greater ABC transporter activation than larger size QDs (Huang et al. 2019).

The endocytic pathway may determine the fate of QDs in the cell and subsequent degradation or release from the cell. We were interested to analyze the endocytic pathway of QD uptake in MSCs. Importantly, it was observed that the uptake pathway depends on the presence or absence of FBS. In a serum-containing medium, the addition of CPZ decreased the QD uptake (Fig. 14, A, C). CPZ is clathrin-mediated endocytosis inhibitor. The inhibition is induced through the anchoring of the clathrin and adapter protein 2 complex to endosomes thereby preventing the assembly of coated pits at the inner plasma membrane (Wang et al. 1993). In a serum-free medium, QD uptake was decreased by both CPZ and nystatin (Fig. 14, B, D). Nystatin is an inhibitor of caveolin/lipid raft mediated endocytosis, which disassembles caveolae and cholesterol in the membrane, but does not interfere with clathrin-mediated endocytosis (Zhu et al. 2011). It has been reported that QDs, possessing a protein corona, are differently recognized by mouse embryonic fibroblast cells NIH3T3 and internalized by different pathways (Damalakiene et al. 2015), consistent with the data from our study. We have shown that NP uptake in MSCs is an active process and does not occur passively. For the development of cell-bases tumor-targeting therapies, elucidation of the endocytic pathway is important to understand the effect and fate of QDs or QD-linked drugs within the cell. To summarize, we have shown that carboxyl-coated QD655 are biocompatible with skin-derived

MSCs. The proliferation, immunophenotype and multipotency of MSCs were not changed by the QD accumulation in the cells. In the presence of serum, QDs were internalized through clathrin-mediated endocytosis, whereas in the absence of serum endocytosis occurred through clathrin and caveolin/lipid raft pathways. The loss of QD signal over time may be explained by the excretion of QDs from MSCs, which could favor the use of MSCs as drug delivery vectors. These data validate the potential use of skin MSCs as NP delivery vectors for tumor-targeted therapies.

### 4.2.2. QD655 delivery to breast cancer cells by nano-engineered mesenchymal stem cells in a three-dimensional co-culture model

Using the data of the optimal QD labelling conditions in MSCs, we established a 3D culture model by growing MSCs in polyHEMA coated cell culture dishes, which prevent the cell adhesion and promotes the aggregation of cells into spheroids which increase in diameter over time (Fig. 15). The cell morphology and even phenotype changes in 3D culture compared to a 2D culture. We evaluated cell viability in a 3D culture to make sure that this does not interfere with the study. An increase in spheroid diameter resulted in a decreased cell viability after 48 h (Fig. 18). Cell viability decrease due to the limited access to oxygen and nutrients in the spheroid core (Langan et al. 2016). Metastatic cancer cells are resistant to extracellular matrix detachment-induced apoptosis, therefore they display better survival and behavior in a 3D culture (Malin et al. 2015). It was demonstrated by our results that MDA-MB-231 were better at surviving in 3D conditions comparing to MCF7 cells (Fig. 18). Similarly, MDA-MB-231 cells were more efficient at QD uptake under 3D conditions comparing to 2D conditions (Fig. 17, B). It has been reported that metastatic breast cancer cells demonstrate a higher nanocarrier uptake efficiency due to the overexpression of integrin receptors which mediate the uptake of NPs through integrin receptor-mediated endocytosis (Murugan et al. 2016).

We observed a decrease in CD90 expression in MSCs after 48 h propagation in 3D conditions. This could be explained by a cell reaction to the change in the microenvironment or cell differentiation (Wiesmann et al. 2006, Lee et al. 2009). To be able to distinguish cells in a 3D co-culture settings, we had to use a selective marker for one of the cell types. CD90 is one of the main markers used for MSC characterization while in breast cancer cells MDA-MB-231 and MCF7 this marker is absent (Riekstina et al. 2009, Lobba et al. 2012). EpCAM is reported to be highly expressed in MCF-7 cells while it is low expressed in MDA-MB-231 cells (Martowicz et al. 2012, Shigdar et al. 2013). We chose CD90 as an MSC marker and EpCAM as an MCF7 marker for the

3D co-culture. It has been reported that a slight CD90 expression can be induced in cancer cells after 48-72 h of co-culture with MSCs and EpCAM expression can be induced in MSCs after 72 h co-culture with cancer cells (Mandel et al. 2013, Yang et al. 2015). However, such a marker induction has not been reported during a 24 h incubation period, therefore it was chosen as an optimal co-culture time.

Next we generated a co-culture of QD-loaded skin MSCs and non-metastatic breast cancer cells MCF7 or metastatic breast cancer cells MDA-MB-231. Flow cytometry and immunofluorescence analysis confirmed that QDs from nano-engineered MSCs can be transferred to breast cancer cells after 24 h co-culture (Fig. 19-21). Interestingly, approximately three times higher transfer efficiency was observed to metastatic breast cancer cell line MDA-MB-231 comparing to non-metastatic cells MCF7 (Fig. 19). Our colleagues from prof. Rotomskis group at National Cancer Institute, Vilnius, Lithuania, demonstrated the same approach in breast cancer-bearing mice. They observed that the main accumulation of QDs in present at the tumor site at 24 h and seven days' post-administration of cells. After seven days the amount of QDs at metastasis sites increased indicating that QDs can be brought to metastasis also *in vivo*. The clearance of QDs was observed through spleen and kidneys (Dapkute et al. 2017). Cell-cell contacts are crucial for the NP delivery to tumors. Nanotube formation and cell-cell fusion is reported to be the mechanism of QD transfer between MSCs and breast cancer cells (Yang et al. 2015, Melzer et al. 2016)

In summary, we have demonstrated the feasibility of a 3D co-culture model to study targeted drug delivery by nano-engineered MSCs. For NP delivery purposes, MSC labelling with QDs in serum-free medium ensures an increased loading efficiency. The QD transfer from MSCs is more efficient in co-culture with the metastatic breast cancer cell line MDA-MB-231 compared with primary breast cancer cell line MCF7. Thus, nano-engineered MSCs could be considered as NP delivery vehicles to specifically target metastatic breast cancer cells.

### 4.3. Use of natural compounds for modulation of mesenchymal stem cell differentiation

Anthocyanidins are compounds belonging to the polyphenol class of phytochemicals. They are the sugar-free counterparts of anthocyanins (Li et al. 2017). They are present in many foods and particularly in berries (Khoo et al. 2017). Different plant extracts and bioactive plant-derived molecules are tested for their effects on MSCs (Saud et al. 2019). Up to date no studies have been conducted to analyze how anthocyanidins impact adipose tissue-derived MSC differentiation. For this study malvidin, cyanidin and delphinidin were chosen. For this study we chose malvidin,

cyanidin and delphinidin. We selected liraglutide as a reference drug, because it is used as a diabetes *mellitus* and anti-obesity drug which reduces intracellular lipid accumulation (Cantini et al. 2015). Liraglutide is investigated also for treatment of osteoporosis and osteoarthritis (Wen et al. 2018, Mei et al. 2019) and therefore served as a reference for all three differentiation experiments.

We observed that addition of malvidin and cyanidin to the adipogenesis differentiation medium, increased the expression of adipocyte related genes *Adiponectin, FABP4* and *LPL* while delphinidin exerted an opposite effect inhibiting *FABP4* expression and decreasing the expression tendency in *Adiponectin* and *LPL* transcripts (Fig. 23). Importantly, delphinidin effects were comparable to liraglutide effects. Anthocyanins from grape extract have shown to inhibit lipogenesis during adipocyte differentiation of mouse embryonic fibroblast cells 3T3-L1. It was characterized by a decreased accumulation of triglycerides and downregulation of lipogenic transcription factors (Lee et al. 2014). Similarly, anthocyanin extracts from fruit of *Vitis coignetiae* have shown an attenuated adipodifferentiation from 3T3-L1 cells confirmed by the decrease of lipid droplets, lipid content, triglyceride production and inhibition of adipogenic transcription factors. This regulation is associated with the activation of AMP-activated protein kinase signaling pathway (Han et al. 2018). The whole anthocyanin fraction from fruit extracts was used in these studies, therefore no conclusions can be made on the effect of individual components. Since delphinidin is one of the components in fruit anthocyanin fraction, we could propose that it promotes the adipogenesis inhibitory effect. The use of berry supplements for overweight patients has been tested in clinical trials. It has been shown that higher intake of food rich in flavonols, flavan-3-ols, anthocyanins and flavonoid polymers was associated with weight loss in adulthood (Bertoia et al. 2016). Delphinidin-rich berry extracts decreased blood glucose and increased insulin levels in prediabetic humans, thus indicating a promising strategy for diabetes prevention (Alvarado et al. 2016). Literature data together with our results indicate that delphinidin could be further investigated as a natural antiobesity or type II diabetes prophylactic or therapeutic agent.

Next, we investigated the impact of anthocyanidins on the osteodifferentiation of adipose tissue-derived MSCs. We demonstrated that malvidin significantly upregulated the expression of osteoblast marker genes (*Runx-2*, *BMP-2),* BMP-2 protein secretion and improved calcium accumulation in differentiated MSCs (Fig. 24, B). A similar effect was observed by liraglutide which upregulated the expression of *BMP-2* gene and protein expression. Glucagon-like peptide 1 (GLP-1) receptor plays a role in bone tissue disorders, therefore its agonists could serve as

promising drugs for diseases like osteoporosis. It is known that GLP-1 enhances bone mineral density, improves bone quality, promotes bone formation and inhibits bone resorption (Zhao et al. 2017). Delphinidin has shown to prevent bone loss through the inhibition of osteoclastogenesis in osteoporosis model mice (Moriwaki et al. 2014). Up to date, we are first to report that malvidin exerts osteodifferentiation stimulating effect similar to liraglutide in MSCs. Malvidin effects as a natural bone protective prophylactic or therapeutic agent should be further investigated to get a better understanding of the underlying mechanisms.

The use of anthocyanidins was tested also on chondrodifferentiation of adipose tissue-derived MSCs. We observed that cyanidin and delphinidin increased the expression of chondrocyte markers *Col2a1* and *Aggrecan.* Similarly did liraglutide (Fig. 25, C, D). Malvidin however exerted no significant effect on chondrocyte specific markers. Delphinidin also increased the accumulation of glycosaminoglycans (Fig. 25, G). It has been previously reported that cyanidin inhibits MSC differentiation into hypertrophic chondrocytes through the suppression of cell autophagic activity (Cao et al. 2018). Cyanidin containing raspberry extract possesses anti-inflammatory properties and decreases the incidence and severity of arthritis *in vivo* (Jean-Gilles et al. 2012). Delphinidin and malvidin are reported to inhibit the production of cartilage-degrading molecule prostaglandin E2 ($PGE_2$) in human chondrocytes and osteoarthritic rats (Haseeb et al. 2013, Dai et al. 2017). Our study demonstrates that anthocyanidin treatment does not induce the formation of hypertrophic chondrocytes from MSCs which is confirmed by unchanged *Runx2* and *BMP-2* expression and BMP-2 secretion (Fig. 25). The role of GLP-1 receptor in osteoarthritis has been recently reported. Liraglutide is shown to diminish cartilage degeneration in osteoarthritic rats *in vivo* (Chen et al. 2018). These data suggest that cyanidin and delphinidin exert similar effects to liraglutide during MSC chondrogenesis and, therefore they should be further investigated as natural prophylactic and therapeutic agents for the strengthening of cartilage in cartilage pathologies and osteoarthritis.

Mutual regulation between adipocytes and osteoblasts during MSC differentiation has been reported by other studies. Chemical, physical and biological factors activate different signaling pathways and various transcription factors that guide MSCs to commit to either lineage (Chen et al. 2016). Runx2 in MSCs promote differentiation into immature osteoblasts, while inhibits lineage commitment to the adipocytes (Komori 2010). Different chemical factors can act as switches between both fates. Isobutylmethylxanthine, dexamethasone and insulin are used to initiate MCS adipogenesis, while L-ascorbic acid and β-glycerophosphate are used to induce MSC osteodifferentiation (Pittenger et al. 1999, Ren et al. 2008). We observed that cyanidin significantly

induces adipocyte marker gene expression, while downregulates calcium accumulation in MSCs after osteodifferentiation. This opposite effect indicates that cyanidin could impact signaling pathways involved in MCS fate decision. Therefore, its use for therapeutic purpose in osteoarthritis should be carefully investigated to understand the underlying mechanisms of its action and possible interference with MCS osteodifferentiation.

Due to health benefits, phytochemicals from plants generate a lot of interest, demanding further scientific evaluation. Extracts from various plants have shown to promote osteodifferentiation and even neurogenic differentiation. MSCs along with medicinal plant extracts have a potential for regenerative therapy. Natural bioactive compounds produce less toxic side effects, are affordable and can increase the disease treating capacity (Saud et al. 2019).

To summarize, individual structural features of anthocyanidins determine their different influences on MSC adipogenesis, osteogenesis and chondrogenesis. Delphinidin inhibits adipogenesis similarly to the anti-obesity and diabetes drug liraglutide. Malvidin promotes MSC osteogenesis by the upregulation of bone developmental markers. Cyanidin and delphinidin stimulate MSC chondrogenesis by promoting the upregulation of chondrocyte structural markers. Anthocyanidins exert anti-obesity and stem cell differentiation promoting effects that could be further studied *in vivo* to verify their potential in anti-obesity, osteoarthritis and osteoporosis treatment.

# 5. CONCLUSIONS

1. A robust and feasible *in vitro* model to study mesenchymal stem cell differentiation into Schwann cell phenotype was established;
2. The developed Schwann cell differentiation model was suitable for screening the effect of sigma 1 receptor ligands on Schwann cells. The sigma 1 receptor antagonist NE-100 showed the inhibition of MBP expression in Schwann cell-like cells;
3. A three-dimensional *in vitro* model to study the nanoparticle delivery to cancer cells by mesenchymal stem cells was established;
4. Using the established nanoparticle delivery model, higher nanoparticle delivery efficiency was observed to metastatic breast cancer cell MDA-MB-231 line compared to primary breast cancer MCF-7 cell line;
5. Mesenchymal stem cell trilineage differentiation *in vitro* model is useful to study the effect of natural compounds on adipogenesis, osteogenesis and chondrogenesis;
6. The effects of three anthocyanidins were elucidated in the MSC trilineage differentiation model. Delphinidin inhibited adipogenesis, malvidin promoted osteogenesis, delphinidin and cyanidin stimulated chondrogenesis;
7. MSC plasticity and easy propagation *in vitro* are excellent properties that can be explored in a large variety of model systems to study the effects of pharmacologically active compounds on adult stem cells.

# 6. SCIENTIFIC PUBLICATIONS AND CONFERENCE PRESENTATIONS

**Scientific publications:**

- **L. Saulite,** D. Dapkute, K. Pleiko, I. Popena, S. Steponkiene, R. Rotomskis, U. Riekstina. Nano-engineered skin mesenchymal stem cells: potential vehicles for tumour targeted quantum dot delivery. *Beilstein Journal of Nanotechnology*, 2017, 8, p. 1218-1230, **doi:10.3762/bjnano.8.123**

- **L. Saulite**, E. Vavers, L. Zvejniece, M. Dambrova, U. Riekstina. The Differentiation of Skin Mesenchymal Stem Cells Towards a Schwann Cell Phenotype: Impact of Sigma-1 Receptor Activation. *Molecular Neurobiology*, 2018, 4, 2840-2850. **doi:10.1007/s12035-017-0511-9**

- **L. Saulite,** K. Pleiko, I. Popena, D. Dapkute, R. Rotomskis, U. Riekstina. Nanoparticle delivery to metastatic breast cancer cells by nano-engineered mesenchymal stem cells. *Beilstein J. Nanotechnol*. 2018, 9, 321-332, **doi:10.3762/bjnano.9.32**.

- **L. Saulite**, K. Jekabsons, M. Klavins, R. Muceniece, U. Riekstina. Malvidin, cyanidin and delphinidin exert diverse effects on human adipose mesenchymal stem cell differentiation. *Phytomedicine, 2019, 53, 86-95.* **doi:https://doi.org/10.1016/j.phymed.2018.09.029**

**Poster presentations at international scientific conferences:**

- **L. Saulite**, E. Vavers, L. Zvejniece, V. Parfejevs, M. Dambrova, U. Riekstina. Sigma-1 receptor ligand effect on the differentiation of skin mesenchymal stem cells towards myelinating Schwann cells. 2nd European Symposium on Physiopathology of sigma-1 receptors, 2019, May 31 - June 2, Riga, Latvia.

- **L. Saulite,** K. Jekabsons, M. Klavins, R. Mucenience, U. Riekstina. Anthocyanidins and anti-obesity drug liraglutide promote human adipose mesenchymal cell differentiation into

chondrocyte and osteocyte lineages. International Pharma Conference and Expo, May 2-4, 2018, Rome, Italy.

- **L. Saulite**, K. Jekabsons, I. Popena, R. Muceniece, M. Klavins, U. Riekstina. Influence of anthocyanins on the adipogenic and chondrogenic differentiation of human adipose mesenchymal stem cells. 2nd International Conference in Pharmacology: From Cellular Processes to Drug Targets (ICP2017RIGA), Riga, Latvia, October 19-20, 2017.

- U. Riekstina, D. Dapkute, **L. Saulite**, K. Jekabsons, I. Popena, K. Pleiko, S. Steponkiene, R. Rotomskis. Characterization of Qdot655 carboxyl uptake and functional effects on human mesenchymal stem cells. 2nd International Conference "Current Trends of Cancer Theranostics (CTCT2016), Druskininkai, Lithuania, June 19-22, 2016.

- **L. Saulite,** E. Vavers, L. Zvejniece, M. Dambrova, U. Riekstina. Sigma-1 receptor ligands impact the differentiation of skin mesenchymal stem cells towards Schwann cell phenotype. The 2015 Tissue Engineering Congress, London, United Kingdom, September 8-10, 2015.

- **L. Saulite**, E. Vavers, L. Zvejniece, M. Dambrova, U. Riekstina. SigmaR1 ligands impact the neurodifferentiation of skin mesenchymal stem cells. Drug Discovery conference, Riga, Latvia, August 27-29, 2015.

**Selected oral presentations at international scientific conferences:**

- **L. Saulite**, K. Jekabsons, U. Riekstina, M. Klavins, R. Muceniece. Impact of anthocyanidins on the differentiation capacity of human adipose mesenchymal stem cells. 76th International Scientific conference of the University of Latvia, Riga, Latvia, February 23, 2018.
- **L. Saulite**. Skin derived MSCs as tool for cell-based therapy research. III annual International conference of Lithuanian Stem Cell Research Association. Vilnius, Lithuania, October 27, 2017.

- **L. Saulite**, D. Dapkute, S. Pluduma, R. Rotomskis, U. Riekstina. Quantum dot transfer from mesenchymal stem cells to breast cancer cells in a 3D co-culture model. 75th International Scientific conference of the University of Latvia, Riga, Latvia, February 24, 2017.

# 7. ACKNOWLEDGMENTS

I wish to express my greatest gratitude to my supervisor prof. Dr. Una Riekstina who inspired, motivated and supported me throughout the years of work and studies at the Faculty of Medicine. I am thankful to my close colleagues Karlis Pleiko, Kaspars Jekabsons, Vadims Parfejevs, Karina Narbute, Jana Namniece, Ineta Popena for creating a great atmosphere at work and helping with scientific and non-scientific questions. I express gratitude to prof. Dr. Ruta Muceniece who involved me in an interesting research and always believed in my abilities.

I thank my parents and sister for eternal support and encouragement to pursue a carrier in life sciences. I am grateful to my beloved husband Kristaps for love and enormous support during my career-related activities.

## 8. REFERENCES


Abbasi-Kangevari, M., et al. (2019). "Potential Therapeutic Features of Human Amniotic Mesenchymal Stem Cells in Multiple Sclerosis: Immunomodulation, Inflammation Suppression, Angiogenesis Promotion, Oxidative Stress Inhibition, Neurogenesis Induction, MMPs Regulation, and Remyelination Stimulation." *Front Immunol* 10: 238. DOI: 10.3389/fimmu.2019.00238.

Abdelkhaliq, A., et al. (2018). "Impact of nanoparticle surface functionalization on the protein corona and cellular adhesion, uptake and transport." *J Nanobiotechnology* 16(1): 70. DOI: 10.1186/s12951-018-0394-6.

Alvarado, J. L., et al. (2016). "Delphinidin-Rich Maqui Berry Extract (Delphinol(R)) Lowers Fasting and Postprandial Glycemia and Insulinemia in Prediabetic Individuals during Oral Glucose Tolerance Tests." *Biomed Res Int* 2016: 1-10. DOI: 10.1155/2016/9070537.

Andrzejewska, A., et al. (2019). "Concise Review: Mesenchymal Stem Cells: From Roots to Boost." *Stem Cells* 37(7): 855-864. DOI: 10.1002/stem.3016.

Anghileri, E., et al. (2008). "Neuronal differentiation potential of human adipose-derived mesenchymal stem cells." *Stem Cells Dev* 17(5): 909-916. DOI: 10.1089/scd.2007.0197.

Baxter-Holland, M. and C. R. Dass (2018). "Doxorubicin, mesenchymal stem cell toxicity and antitumour activity: implications for clinical use." *J Pharm Pharmacol* 70(3): 320-327. DOI: 10.1111/jphp.12869.

Bertoia, M. L., et al. (2016). "Dietary flavonoid intake and weight maintenance: three prospective cohorts of 124,086 US men and women followed for up to 24 years." *BMJ* 352: i17. DOI: 10.1136/bmj.i17.

Biernaskie, J. A., et al. (2006). "Isolation of skin-derived precursors (SKPs) and differentiation and enrichment of their Schwann cell progeny." *Nat Protoc* 1(6): 2803-2812. DOI: 10.1038/nprot.2006.422.

Bogdanowicz, D. R. and H. H. Lu (2017). "Designing the stem cell microenvironment for guided connective tissue regeneration." *Ann N Y Acad Sci* 1410(1): 3-25. DOI: 10.1111/nyas.13553.

Bruno, S., et al. (2013). "Microvesicles derived from human bone marrow mesenchymal stem cells inhibit tumor growth." *Stem Cells Dev* 22(5): 758-771. DOI: 10.1089/scd.2012.0304.

Buckwalter, J. A., et al. (2000). "Synovial joint degeneration and the syndrome of osteoarthritis." *Instr Course Lect* 49: 481-489.

Cantini, G., et al. (2015). "Effect of liraglutide on proliferation and differentiation of human adipose stem cells." *Mol Cell Endocrinol* 402: 43-50. DOI: 10.1016/j.mce.2014.12.021.

Cao, S., et al. (2018). "Nano-loaded human umbilical cord mesenchymal stem cells as targeted carriers of doxorubicin for breast cancer therapy." *Artif Cells Nanomed Biotechnol* 46(sup1): 642-652. DOI: 10.1080/21691401.2018.1434185.

Cao, Z., et al. (2018). "Cyanidin suppresses autophagic activity regulating chondrocyte hypertrophic differentiation." *J Cell Physiol* 233(3): 2332-2342. DOI: 10.1002/jcp.26105.

Caplan, A. I. (1991). "Mesenchymal stem cells." *J Orthop Res* 9(5): 641-650. DOI: 10.1002/jor.1100090504.

Caplan, A. I. (2018). "Cell-Based Therapies: The Nonresponder." *Stem Cells Transl Med* 7(11): 762-766. DOI: 10.1002/sctm.18-0074.

Chan, T. S., et al. (2019). "Targeting the Interplay Between Cancer Fibroblasts, Mesenchymal Stem Cells, and Cancer Stem Cells in Desmoplastic Cancers." *Front Oncol* 9: 688. DOI: 10.3389/fonc.2019.00688.

Chen, D., et al. (2015). "Transdifferentiation of Umbilical Cord-Derived Mesenchymal Stem Cells Into Epidermal-Like Cells by the Mimicking Skin Microenvironment." *Int J Low Extrem Wounds* 14(2): 136-145. DOI: 10.1177/1534734615569913.

Chen, J., et al. (2018). "Glucagon-like peptide-1 receptor regulates endoplasmic reticulum stress-induced apoptosis and the associated inflammatory response in chondrocytes and the progression of osteoarthritis in rat." *Cell Death Dis* 9(2): 1-14. DOI: 10.1038/s41419-017-0217-y.

Chen, J., et al. (2017). "GLP-1/GLP-1R Signaling in Regulation of Adipocyte Differentiation and Lipogenesis." *Cell Physiol Biochem* 42(3): 1165-1176. DOI: 10.1159/000478872.

Chen, Q., et al. (2016). "Fate decision of mesenchymal stem cells: adipocytes or osteoblasts?" *Cell Death Differ* 23(7): 1128-1139. DOI: 10.1038/cdd.2015.168.

Chen, T., et al. (2011). "Smart multifunctional nanostructure for targeted cancer chemotherapy and magnetic resonance imaging." *ACS Nano* 5(10): 7866-7873. DOI: 10.1021/nn202073m.

Chulpanova, D. S., et al. (2018). "Application of Mesenchymal Stem Cells for Therapeutic Agent Delivery in Anti-tumor Treatment." *Front Pharmacol* 9: 259. DOI: 10.3389/fphar.2018.00259.

Colpo, G. D., et al. (2015). "Mesenchymal stem cells for the treatment of neurodegenerative and psychiatric disorders." *An Acad Bras Cienc* 87(2 Suppl): 1435-1449. DOI: 10.1590/0001-3765201520140619.

Cooney, D. S., et al. (2016). "Mesenchymal Stem Cells Enhance Nerve Regeneration in a Rat Sciatic Nerve Repair and Hindlimb Transplant Model." *Sci Rep* 6: 31306. DOI: 10.1038/srep31306.

Cruz-Martinez, P., et al. (2016). "Intraventricular injections of mesenchymal stem cells activate endogenous functional remyelination in a chronic demyelinating murine model." *Cell Death Dis* 7: e2223. DOI: 10.1038/cddis.2016.130.

Dai, T., et al. (2017). "Malvidin attenuates pain and inflammation in rats with osteoarthritis by suppressing NF-kappaB signaling pathway." *Inflamm Res* 66(12): 1075-1084. DOI: 10.1007/s00011-017-1087-6.

Damalakiene, L., et al. (2015). "Suppression of a Specific Intracellular Uptake Pathway by a Saturating Accumulation of Quantum Dots." *J Biomed Nanotechnol* 11(5): 841-853.

Dapkute, D., et al. (2017). "Skin-derived mesenchymal stem cells as quantum dot vehicles to tumors." *Int J Nanomedicine* 12: 8129-8142. DOI: 10.2147/IJN.S143367.

de la Torre, P., et al. (2020). "Cell-Based Nanoparticles Delivery Systems for Targeted Cancer Therapy: Lessons from Anti-Angiogenesis Treatments." *Molecules* 25(3). DOI: 10.3390/molecules25030715.

Dean, M. (2009). "ABC transporters, drug resistance, and cancer stem cells." *J Mammary Gland Biol Neoplasia* 14(1): 3-9. DOI: 10.1007/s10911-009-9109-9.

Decambron, A., et al. (2017). "Low-dose BMP-2 and MSC dual delivery onto coral scaffold for critical-size bone defect regeneration in sheep." *J Orthop Res* 35(12): 2637-2645. DOI: 10.1002/jor.23577.

Dominici, M., et al. (2006). "Minimal criteria for defining multipotent mesenchymal stromal cells. The International Society for Cellular Therapy position statement." *Cytotherapy* 8(4): 315-317. DOI: 10.1080/14653240600855905.

Faroni, A., et al. (2016). "Human Schwann-like cells derived from adipose-derived mesenchymal stem cells rapidly de-differentiate in the absence of stimulating medium." *Eur J Neurosci* 43(3): 417-430. DOI: 10.1111/ejn.13055.

Ferreira, J. R., et al. (2018). "Mesenchymal Stromal Cell Secretome: Influencing Therapeutic Potential by Cellular Pre-conditioning." *Front Immunol* 9: 2837. DOI: 10.3389/fimmu.2018.02837.

Foudah, D., et al. (2014). "Expression of neural markers by undifferentiated mesenchymal-like stem cells from different sources." *J Immunol Res* 2014: 987678. DOI: 10.1155/2014/987678.

Friedenstein, A. J., et al. (1970). "The development of fibroblast colonies in monolayer cultures of guinea-pig bone marrow and spleen cells." *Cell Tissue Kinet* 3(4): 393-403. DOI: 10.1111/j.1365-2184.1970.tb00347.x.

Friedenstein, A. J., et al. (1966). "Osteogenesis in transplants of bone marrow cells." *J Embryol Exp Morphol* 16(3): 381-390.

Fu, X., et al. (2019). "Mesenchymal Stem Cell Migration and Tissue Repair." *Cells* 8(8). DOI: 10.3390/cells8080784.

Grayson, W. L., et al. (2015). "Stromal cells and stem cells in clinical bone regeneration." *Nat Rev Endocrinol* 11(3): 140-150. DOI: 10.1038/nrendo.2014.234.

Grisendi, G., et al. (2015). "Mesenchymal progenitors expressing TRAIL induce apoptosis in sarcomas." *Stem Cells* 33(3): 859-869. DOI: 10.1002/stem.1903.

Habibovic, P. (2017). "(*) Strategic Directions in Osteoinduction and Biomimetics." *Tissue Eng Part A* 23(23-24): 1295-1296. DOI: 10.1089/ten.TEA.2017.0430.

Hayashi, T. (2015). "Sigma-1 receptor: the novel intracellular target of neuropsychotherapeutic drugs." *J Pharmacol Sci* 127(1): 2-5. DOI: 10.1016/j.jphs.2014.07.001.

Hayashi, T. and T. P. Su (2004). "Sigma-1 receptors at galactosylceramide-enriched lipid microdomains regulate oligodendrocyte differentiation." *Proc Natl Acad Sci U S A* 101(41): 14949-14954. DOI: 10.1073/pnas.0402890101.

Hayashi, T. and T. P. Su (2007). "Sigma-1 receptor chaperones at the ER-mitochondrion interface regulate Ca(2+) signaling and cell survival." *Cell* 131(3): 596-610. DOI: 10.1016/j.cell.2007.08.036.

Han, M. H., et al. (2018). "Inhibition of Adipocyte Differentiation by Anthocyanins Isolated from the Fruit of Vitis coignetiae Pulliat is Associated with the Activation of AMPK Signaling Pathway." *Toxicol Res* 34(1): 13-21. DOI: 10.5487/TR.2018.34.1.013.

Harrell, C. R., et al. (2019). "Molecular Mechanisms Responsible for Therapeutic Potential of Mesenchymal Stem Cell-Derived Secretome." *Cells* 8(5). DOI: 10.3390/cells8050467.

Haseeb, A., et al. (2013). "Delphinidin inhibits IL-1beta-induced activation of NF-kappaB by modulating the phosphorylation of IRAK-1(Ser376) in human articular chondrocytes." *Rheumatology* 52(6): 998-1008. DOI: 10.1093/rheumatology/kes363.

Hass, R., et al. (2011). "Different populations and sources of human mesenchymal stem cells (MSC): A comparison of adult and neonatal tissue-derived MSC." *Cell Commun Signal* 9: 12. DOI: 10.1186/1478-811X-9-12.

Herberts, C. A., et al. (2011). "Risk factors in the development of stem cell therapy." *J Transl Med* 9: 29. DOI: 10.1186/1479-5876-9-29.

Hoogduijn, M. J. and E. Lombardo (2019). "Mesenchymal Stromal Cells Anno 2019: Dawn of the Therapeutic Era? Concise Review." *Stem Cells Transl Med* 8(11): 1126-1134. DOI: 10.1002/sctm.19-0073.

Huang, G., et al. (2019). "Involvement of ABC transporters in the efflux and toxicity of MPA-COOH-CdTe quantum dots in human breast cancer SK-BR-3 cells." *J Biochem Mol Toxicol* 33(8): e22343. DOI: 10.1002/jbt.22343.

Huang, L., et al. (2019). "Intercellular Crosstalk of Mesenchymal Stem Cells with Prostate Cancer Cells via Microvesicles Loaded with Magnetic Nanocubes for Targeted Magnetic Hyperthermia." *J Biomed Nanotechnol* 15(12): 2291-2304. DOI: 10.1166/jbn.2019.2868.

Iaquinta, M. R., et al. (2019). "Adult Stem Cells for Bone Regeneration and Repair." *Front Cell Dev Biol* 7: 268. DOI: 10.3389/fcell.2019.00268.

Yamagata, K., et al. (2018). "Use of mesenchymal stem cells seeded on the scaffold in articular cartilage repair." *Inflamm Regen* 38: 4. DOI: 10.1186/s41232-018-0061-1.

Yang, Y., et al. (2015). "Human mesenchymal stroma/stem cells exchange membrane proteins and alter functionality during interaction with different tumor cell lines." *Stem Cells Dev* 24(10): 1205-1222. DOI: 10.1089/scd.2014.0413.

Jean-Gilles, D., et al. (2012). "Anti-inflammatory effects of polyphenolic-enriched red raspberry extract in an antigen-induced arthritis rat model." *J Agric Food Chem* 60(23): 5755-5762. DOI: 10.1021/jf203456w.

Jessen, K. R. and R. Mirsky (2016). "The repair Schwann cell and its function in regenerating nerves." *J Physiol* 594(13): 3521-3531. DOI: 10.1113/JP270874.

Jessen, K. R. and R. Mirsky (2019). "The Success and Failure of the Schwann Cell Response to Nerve Injury." *Front Cell Neurosci* 13: 33. DOI: 10.3389/fncel.2019.00033.

Jessen, K. R., et al. (2015). "Schwann Cells: Development and Role in Nerve Repair." *Cold Spring Harb Perspect Biol* 7(7): a020487. DOI: 10.1101/cshperspect.a020487.

Kabashima-Niibe, A., et al. (2013). "Mesenchymal stem cells regulate epithelial-mesenchymal transition and tumor progression of pancreatic cancer cells." *Cancer Sci* 104(2): 157-164. DOI: 10.1111/cas.12059.

Kalvins I, L. A., Cernobrovijs A, Dambrova M, Zvejniece L, Vorona M, Veinbergs G (2011). "4R,5S-enantiomer of 2-(5-methyl-2-oxo-4-phenyl-pyrrolidin-1-yl)-acetamide with nootropic activity." *WO2011054888 (A1)*.

Khoo, H. E., et al. (2017). "Anthocyanidins and anthocyanins: colored pigments as food, pharmaceutical ingredients, and the potential health benefits." *Food Nutr Res* 61(1): 2-21. DOI: 10.1080/16546628.2017.1361779.

Kim, N. and S. G. Cho (2013). "Clinical applications of mesenchymal stem cells." *Korean J Intern Med* 28(4): 387-402. DOI: 10.3904/kjim.2013.28.4.387.

Kim, S. M., et al. (2010). "Irradiation enhances the tumor tropism and therapeutic potential of tumor necrosis factor-related apoptosis-inducing ligand-secreting human umbilical cord blood-derived mesenchymal stem cells in glioma therapy." *Stem Cells* 28(12): 2217-2228. DOI: 10.1002/stem.543.

Klopp, A. H., et al. (2007). "Tumor irradiation increases the recruitment of circulating mesenchymal stem cells into the tumor microenvironment." *Cancer Res* 67(24): 11687-11695. DOI: 10.1158/0008-5472.CAN-07-1406.

Komori, T. (2010). "Regulation of osteoblast differentiation by Runx2." *Adv Exp Med Biol* 658: 43-49. DOI: 10.1007/978-1-4419-1050-9_5.

Krueger, T. E. G., et al. (2018). "Concise Review: Mesenchymal Stem Cell-Based Drug Delivery: The Good, the Bad, the Ugly, and the Promise." *Stem Cells Transl Med* 7(9): 651-663. DOI: 10.1002/sctm.18-0024.

Kuroda, Y., et al. (2013). "Isolation, culture and evaluation of multilineage-differentiating stress-enduring (Muse) cells." *Nat Protoc* 8(7): 1391-1415. DOI: 10.1038/nprot.2013.076.

Kusadasi, N. and A. B. Groeneveld (2013). "A perspective on mesenchymal stromal cell transplantation in the treatment of sepsis." *Shock* 40(5): 352-357. DOI: 10.1097/SHK.0000000000000039.

Langan, L. M., et al. (2016). "Direct Measurements of Oxygen Gradients in Spheroid Culture System Using Electron Parametric Resonance Oximetry." *PLoS One* 11(2): e0149492. DOI: 10.1371/journal.pone.0149492.

Lazarus, H. M., et al. (1995). "Ex vivo expansion and subsequent infusion of human bone marrow-derived stromal progenitor cells (mesenchymal progenitor cells): implications for therapeutic use." *Bone Marrow Transplant* 16(4): 557-564.

Lee, B., et al. (2014). "Anthocyanins inhibit lipogenesis during adipocyte differentiation of 3T3-L1 preadipocytes." *Plant Foods Hum Nutr* 69(2): 137-141. DOI: 10.1007/s11130-014-0407-z.

Lee, H. J., et al. (2009). "Changes in surface markers of human mesenchymal stem cells during the chondrogenic differentiation and dedifferentiation processes in vitro." *Arthritis Rheum* 60(8): 2325-2332. DOI: 10.1002/art.24786.

Lee, K. B., et al. (2007). "Injectable mesenchymal stem cell therapy for large cartilage defects--a porcine model." *Stem Cells* 25(11): 2964-2971. DOI: 10.1634/stemcells.2006-0311.

Lee, K. D., et al. (2004). "In vitro hepatic differentiation of human mesenchymal stem cells." *Hepatology* 40(6): 1275-1284. DOI: 10.1002/hep.20469.

Lee, M. W., et al. (2019). "Mesenchymal stem cells in suppression or progression of hematologic malignancy: current status and challenges." *Leukemia* 33(3): 597-611. DOI: 10.1038/s41375-018-0373-9.

Li, D., et al. (2017). "Health benefits of anthocyanins and molecular mechanisms: Update from recent decade." *Crit Rev Food Sci Nutr* 57(8): 1729-1741. DOI: 10.1080/10408398.2015.1030064.

Liu, H., et al. (2015). "CdSe/ZnS Quantum Dots-Labeled Mesenchymal Stem Cells for Targeted Fluorescence Imaging of Pancreas Tissues and Therapy of Type 1 Diabetic Rats." *Nanoscale Res Lett* 10(1): 959. DOI: 10.1186/s11671-015-0959-3.

Liu, Z., et al. (2015). "Specific marker expression and cell state of Schwann cells during culture in vitro." *PLoS One* 10(4): e0123278. DOI: 10.1371/journal.pone.0123278.

Livak, K. J. and T. D. Schmittgen (2001). "Analysis of relative gene expression data using real-time quantitative PCR and the 2(-Delta Delta C(T)) Method." *Methods* 25(4): 402-408. DOI: 10.1006/meth.2001.1262.

Lobba, A. R., et al. (2012). "Differential expression of CD90 and CD14 stem cell markers in malignant breast cancer cell lines." *Cytometry A* 81(12): 1084-1091. DOI: 10.1002/cyto.a.22220.

Lv, F. J., et al. (2014). "Concise review: the surface markers and identity of human mesenchymal stem cells." *Stem Cells* 32(6): 1408-1419. DOI: 10.1002/stem.1681.

Malin, D., et al. (2015). "ERK-regulated alphaB-crystallin induction by matrix detachment inhibits anoikis and promotes lung metastasis in vivo." *Oncogene* 34(45): 5626-5634. DOI: 10.1038/onc.2015.12.

Mandel, K., et al. (2013). "Mesenchymal stem cells directly interact with breast cancer cells and promote tumor cell growth in vitro and in vivo." *Stem Cells Dev* 22(23): 3114-3127. DOI: 10.1089/scd.2013.0249.

Martinelli, C., et al. (2019). "Nanostructured carriers as innovative tools for cancer diagnosis and therapy." *APL Bioeng* 3(1): 011502. DOI: 10.1063/1.5079943.

Martowicz, A., et al. (2012). "Phenotype-dependent effects of EpCAM expression on growth and invasion of human breast cancer cell lines." *BMC Cancer* 12: 501. DOI: 10.1186/1471-2407-12-501.

Masgutov, R., et al. (2019). "Adipose-Derived Mesenchymal Stem Cells Applied in Fibrin Glue Stimulate Peripheral Nerve Regeneration." *Front Med (Lausanne)* 6: 68. DOI: 10.3389/fmed.2019.00068.

Mata, M., et al. (1990). "S100 is preferentially distributed in myelin-forming Schwann cells." *J Neurocytol* 19(3): 432-442. DOI: 10.1007/bf01188409.

Matsushita, K. and V. J. Dzau (2017). "Mesenchymal stem cells in obesity: insights for translational applications." *Lab Invest* 97(10): 1158-1166. DOI: 10.1038/labinvest.2017.42.

McGregor, C. E. and A. W. English (2018). "The Role of BDNF in Peripheral Nerve Regeneration: Activity-Dependent Treatments and Val66Met." *Front Cell Neurosci* 12: 522. DOI: 10.3389/fncel.2018.00522.

Mei, J., et al. (2019). "Liraglutide suppresses TNF-alpha-induced degradation of extracellular matrix in human chondrocytes: a therapeutic implication in osteoarthritis." *Am J Transl Res* 11(8): 4800-4808.

Melzer, C., et al. (2016). "Interaction of MSC with tumor cells." *Cell Commun Signal* 14(1): 20. DOI: 10.1186/s12964-016-0143-0.

Moriwaki, S., et al. (2014). "Delphinidin, One of the Major Anthocyanidins, Prevents Bone Loss through the Inhibition of Excessive Osteoclastogenesis in Osteoporosis Model Mice." *Plos One* 9(5): e97177. DOI: ARTN e97177
10.1371/journal.pone.0097177.

Mukhamedshina, Y. O., et al. (2019). "Mesenchymal stem cells and the neuronal microenvironment in the area of spinal cord injury." *Neural Regen Res* 14(2): 227-237. DOI: 10.4103/1673-5374.244778.

Murphy, J. M., et al. (2003). "Stem cell therapy in a caprine model of osteoarthritis." *Arthritis Rheum* 48(12): 3464-3474. DOI: 10.1002/art.11365.

Murugan, C., et al. (2016). "Combinatorial nanocarrier based drug delivery approach for amalgamation of anti-tumor agents in bresat cancer cells: an improved nanomedicine strategies." *Sci Rep* 6: 34053. DOI: 10.1038/srep34053.

Naghdi, M., et al. (2009). "Transdifferentiation of bone marrow stromal cells into cholinergic neuronal phenotype: a potential source for cell therapy in spinal cord injury." *Cytotherapy* 11(2): 137-152. DOI: 10.1080/14653240802716582.

Oh, N. and J. H. Park (2014). "Endocytosis and exocytosis of nanoparticles in mammalian cells." *Int J Nanomedicine* 9 Suppl 1: 51-63. DOI: 10.2147/IJN.S26592.

Olsen, T. R., et al. (2018). "Peak MSC-Are We There Yet?" *Front Med (Lausanne)* 5: 178. DOI: 10.3389/fmed.2018.00178.

Pak, J. (2011). "Regeneration of human bones in hip osteonecrosis and human cartilage in knee osteoarthritis with autologous adipose-tissue-derived stem cells: a case series." *J Med Case Rep* 5: 296. DOI: 10.1186/1752-1947-5-296.

Palacios, G., et al. (2004). "Immunohistochemical localization of the sigma1 receptor in Schwann cells of rat sciatic nerve." *Brain Res* 1007(1-2): 65-70. DOI: 10.1016/j.brainres.2004.02.013.

Paris, J. L., et al. (2019). "Overcoming the stability, toxicity, and biodegradation challenges of tumor stimuli-responsive inorganic nanoparticles for delivery of cancer therapeutics." *Expert Opin Drug Deliv* 16(10): 1095-1112. DOI: 10.1080/17425247.2019.1662786.

Petrou, P., et al. (2016). "Safety and Clinical Effects of Mesenchymal Stem Cells Secreting Neurotrophic Factor Transplantation in Patients With Amyotrophic Lateral Sclerosis: Results of Phase 1/2 and 2a Clinical Trials." *JAMA Neurol* 73(3): 337-344. DOI: 10.1001/jamaneurol.2015.4321.

Phetfong, J., et al. (2016). "Osteoporosis: the current status of mesenchymal stem cell-based therapy." *Cell Mol Biol Lett* 21: 12. DOI: 10.1186/s11658-016-0013-1.

Pi, Q. M., et al. (2010). "Degradation or excretion of quantum dots in mouse embryonic stem cells." *BMC Biotechnol* 10: 36. DOI: 10.1186/1472-6750-10-36.

Pittenger, M. F., et al. (2019). "Mesenchymal stem cell perspective: cell biology to clinical progress." *NPJ Regen Med* 4: 22. DOI: 10.1038/s41536-019-0083-6.

Pittenger, M. F., et al. (1999). "Multilineage potential of adult human mesenchymal stem cells." *Science* 284(5411): 143-147. DOI: 10.1126/science.284.5411.143.

Pucci, C., et al. (2019). "Innovative approaches for cancer treatment: current perspectives and new challenges." *Ecancermedicalscience* 13: 961. DOI: 10.3332/ecancer.2019.961.

Ren, G., et al. (2008). "Mesenchymal stem cell-mediated immunosuppression occurs via concerted action of chemokines and nitric oxide." *Cell Stem Cell* 2(2): 141-150. DOI: 10.1016/j.stem.2007.11.014.

Richardson, S. M., et al. (2010). "Mesenchymal stem cells in regenerative medicine: opportunities and challenges for articular cartilage and intervertebral disc tissue engineering." *J Cell Physiol* 222(1): 23-32. DOI: 10.1002/jcp.21915.

Riekstina, U., et al. (2009). "Embryonic stem cell marker expression pattern in human mesenchymal stem cells derived from bone marrow, adipose tissue, heart and dermis." *Stem Cell Rev* 5(4): 378-386. DOI: 10.1007/s12015-009-9094-9.

Riekstina, U., et al. (2008). "Characterization of human skin-derived mesenchymal stem cell proliferation rate in different growth conditions." *Cytotechnology* 58(3): 153-162. DOI: 10.1007/s10616-009-9183-2.

Rivera, F. J. and L. Aigner (2012). "Adult mesenchymal stem cell therapy for myelin repair in multiple sclerosis." *Biol Res* 45(3): 257-268. DOI: 10.4067/S0716-97602012000300007.

Ryskamp, D. A., et al. (2019). "Neuronal Sigma-1 Receptors: Signaling Functions and Protective Roles in Neurodegenerative Diseases." *Front Neurosci* 13: 862. DOI: 10.3389/fnins.2019.00862.

Romero, L., et al. (2012). "Pharmacological properties of S1RA, a new sigma-1 receptor antagonist that inhibits neuropathic pain and activity-induced spinal sensitization." *Br J Pharmacol* 166(8): 2289-2306. DOI: 10.1111/j.1476-5381.2012.01942.x.

Rossignoli, F., et al. (2019). "Inducible Caspase9-mediated suicide gene for MSC-based cancer gene therapy." *Cancer Gene Ther* 26(1-2): 11-16. DOI: 10.1038/s41417-018-0034-1.

Sacchetti, B., et al. (2016). "No Identical "Mesenchymal Stem Cells" at Different Times and Sites: Human Committed Progenitors of Distinct Origin and Differentiation Potential Are Incorporated as Adventitial Cells in Microvessels." *Stem Cell Reports* 6(6): 897-913. DOI: 10.1016/j.stemcr.2016.05.011.

Saeedi, P., et al. (2019). "A revealing review of mesenchymal stem cells therapy, clinical perspectives and Modification strategies." *Stem Cell Investig* 6: 34. DOI: 10.21037/sci.2019.08.11.

Salinas Tejedor, L., et al. (2015). "Mesenchymal stem cells do not exert direct beneficial effects on CNS remyelination in the absence of the peripheral immune system." *Brain Behav Immun* 50: 155-165. DOI: 10.1016/j.bbi.2015.06.024.

Saud, B., et al. (2019). "A Review on the Effect of Plant Extract on Mesenchymal Stem Cell Proliferation and Differentiation." *Stem Cells Int* 2019: 7513404. DOI: 10.1155/2019/7513404.

Saulite, L., et al. (2018). "The Differentiation of Skin Mesenchymal Stem Cells Towards a Schwann Cell Phenotype: Impact of Sigma-1 Receptor Activation." *Mol Neurobiol* 55(4): 2840-2850. DOI: 10.1007/s12035-017-0511-9.

Sengstock, C., et al. (2014). "Effect of silver nanoparticles on human mesenchymal stem cell differentiation." *Beilstein J Nanotechnol* 5: 2058-2069. DOI: 10.3762/bjnano.5.214.

Shah, N. M., et al. (1994). "Glial growth factor restricts mammalian neural crest stem cells to a glial fate." *Cell* 77(3): 349-360. DOI: 10.1016/0092-8674(94)90150-3.

Shigdar, S., et al. (2013). "The use of sensitive chemical antibodies for diagnosis: detection of low levels of EpCAM in breast cancer." *PLoS One* 8(2): e57613. DOI: 10.1371/journal.pone.0057613.

Shree, N. and R. R. Bhonde (2017). "Conditioned Media From Adipose Tissue Derived Mesenchymal Stem Cells Reverse Insulin Resistance in Cellular Models." *J Cell Biochem* 118(8): 2037-2043. DOI: 10.1002/jcb.25777.

Shree, N., et al. (2019). "Human adipose tissue mesenchymal stem cells as a novel treatment modality for correcting obesity induced metabolic dysregulation." *Int J Obes (Lond)* 43(10): 2107-2118. DOI: 10.1038/s41366-019-0438-5.

Silva, L. H., et al. (2016). "Labeling mesenchymal cells with DMSA-coated gold and iron oxide nanoparticles: assessment of biocompatibility and potential applications." *J Nanobiotechnology* 14(1): 59. DOI: 10.1186/s12951-016-0213-x.

Sonomoto, K., et al. (2016). "Spontaneous Differentiation of Human Mesenchymal Stem Cells on Poly-Lactic-Co-Glycolic Acid Nano-Fiber Scaffold." *PLoS One* 11(4): e0153231. DOI: 10.1371/journal.pone.0153231.

Stolzing, A., et al. (2008). "Age-related changes in human bone marrow-derived mesenchymal stem cells: consequences for cell therapies." *Mech Ageing Dev* 129(3): 163-173. DOI: 10.1016/j.mad.2007.12.002.

Studeny, M., et al. (2002). "Bone marrow-derived mesenchymal stem cells as vehicles for interferon-beta delivery into tumors." *Cancer Res* 62(13): 3603-3608.

Sun, X., et al. (2018). "Differentiation of adipose-derived stem cells into Schwann cell-like cells through intermittent induction: potential advantage of cellular transient memory function." *Stem Cell Res Ther* 9(1): 133. DOI: 10.1186/s13287-018-0884-3.

Takeda, Y. S. and Q. Xu (2015). "Neuronal Differentiation of Human Mesenchymal Stem Cells Using Exosomes Derived from Differentiating Neuronal Cells." *PLoS One* 10(8): e0135111. DOI: 10.1371/journal.pone.0135111.

Tang, X. J., et al. (2014). "TRAIL-engineered bone marrow-derived mesenchymal stem cells: TRAIL expression and cytotoxic effects on C6 glioma cells." *Anticancer Res* 34(2): 729-734.

Tatullo, M., et al. (2015). "Dental pulp stem cells: function, isolation and applications in regenerative medicine." *J Tissue Eng Regen Med* 9(11): 1205-1216. DOI: 10.1002/term.1899.

Ullah, I., et al. (2015). "Human mesenchymal stem cells - current trends and future prospective." *Biosci Rep* 35(2). DOI: 10.1042/BSR20150025.

Urrutia, D. N., et al. (2019). "Comparative study of the neural differentiation capacity of mesenchymal stromal cells from different tissue sources: An approach for their

use in neural regeneration therapies." *PLoS One* 14(3): e0213032. DOI: 10.1371/journal.pone.0213032.

Veinberg, G., et al. (2013). "Synthesis and biological evaluation of 2-(5-methyl-4-phenyl-2-oxopyrrolidin-1-yl)-acetamide stereoisomers as novel positive allosteric modulators of sigma-1 receptor." *Bioorg Med Chem* 21(10): 2764-2771. DOI: 10.1016/j.bmc.2013.03.016.

Ventola, C. L. (2017). "Progress in Nanomedicine: Approved and Investigational Nanodrugs." *P T* 42(12): 742-755.

Viswanathan, S., et al. (2019). "Mesenchymal stem versus stromal cells: International Society for Cell & Gene Therapy (ISCT(R)) Mesenchymal Stromal Cell committee position statement on nomenclature." *Cytotherapy* 21(10): 1019-1024. DOI: 10.1016/j.jcyt.2019.08.002.

Volarevic, V., et al. (2014). "Concise review: Therapeutic potential of mesenchymal stem cells for the treatment of acute liver failure and cirrhosis." *Stem Cells* 32(11): 2818-2823. DOI: 10.1002/stem.1818.

Wakao, S., et al. (2010). "Long-term observation of auto-cell transplantation in non-human primate reveals safety and efficiency of bone marrow stromal cell-derived Schwann cells in peripheral nerve regeneration." *Exp Neurol* 223(2): 537-547. DOI: 10.1016/j.expneurol.2010.01.022.

Walling, M. A., et al. (2009). "Quantum dots for live cell and in vivo imaging." *Int J Mol Sci* 10(2): 441-491. DOI: 10.3390/ijms10020441.

Wang, L. H., et al. (1993). "Mis-assembly of clathrin lattices on endosomes reveals a regulatory switch for coated pit formation." *J Cell Biol* 123(5): 1107-1117.

Wang, W., et al. (2017). "Functional Nanoparticles and their Interactions with Mesenchymal Stem Cells." *Curr Pharm Des* 23(26): 3814-3832. DOI: 10.2174/1381612823666170622110654.

Wang, X., et al. (2018). "Mesenchymal stem cells loaded with paclitaxel-poly(lactic-co-glycolic acid) nanoparticles for glioma-targeting therapy." *Int J Nanomedicine* 13: 5231-5248. DOI: 10.2147/IJN.S167142.

Wang, X., et al. (2018). "The optimal time to inject bone mesenchymal stem cells for fracture healing in a murine model." *Stem Cell Res Ther* 9(1): 272. DOI: 10.1186/s13287-018-1034-7.

Wen, B., et al. (2018). "Liraglutide exerts a bone-protective effect in ovariectomized rats with streptozotocin-induced diabetes by inhibiting osteoclastogenesis." *Exp Ther Med* 15(6): 5077-5083. DOI: 10.3892/etm.2018.6043.

Weng, T. Y., et al. (2017). "Loss of Sigma-1 Receptor Chaperone Promotes Astrocytosis and Enhances the Nrf2 Antioxidant Defense." *Oxid Med Cell Longev* 2017: 4582135. DOI: 10.1155/2017/4582135.

Wicki, A., et al. (2015). "Nanomedicine in cancer therapy: challenges, opportunities, and clinical applications." *J Control Release* 200: 138-157. DOI: 10.1016/j.jconrel.2014.12.030.

Wiesmann, A., et al. (2006). "Decreased CD90 expression in human mesenchymal stem cells by applying mechanical stimulation." *Head Face Med* 2: 8. DOI: 10.1186/1746-160X-2-8.

Xiao, Y. Z. and S. Wang (2015). "Differentiation of Schwannlike cells from human umbilical cord blood mesenchymal stem cells in vitro." *Mol Med Rep* 11(2): 1146-1152. DOI: 10.3892/mmr.2014.2840.

Xu, G., et al. (2016). "The Reproductive Toxicity of CdSe/ZnS Quantum Dots on the in vivo Ovarian Function and in vitro Fertilization." *Sci Rep* 6(37677 ). DOI: 10.1038/srep37677.

Zaminy, A., et al. (2013). "Mesenchymal stem cells as an alternative for Schwann cells in rat spinal cord injury." *Iran Biomed J* 17(3): 113-122. DOI: 10.6091/ibj.1121.2013.

Zhang, R., et al. (2019). "Mesenchymal stem cell related therapies for cartilage lesions and osteoarthritis." *Am J Transl Res* 11(10): 6275-6289.

Zhao, C., et al. (2017). "The Impact of Glucagon-Like Peptide-1 on Bone Metabolism and Its Possible Mechanisms." *Front Endocrinol* 8: 1-8. DOI: 10.3389/fendo.2017.00098.

Zhao, Y., et al. (2017). "Targeted delivery of doxorubicin by nano-loaded mesenchymal stem cells for lung melanoma metastases therapy." *Sci Rep* 7: 44758. DOI: 10.1038/srep44758.

Zhu, X. D., et al. (2011). "Caveolae-dependent Endocytosis Is Required for Class A Macrophage Scavenger Receptor-mediated Apoptosis in Macrophages." *Journal of Biological Chemistry* 286(10): 8231-8239. DOI: 10.1074/jbc.M110.145888.

Zrazhevskiy, P. and X. Gao (2013). "Quantum dot imaging platform for single-cell molecular profiling." *Nat Commun* 4: 1619. DOI: 10.1038/ncomms2635.